C. elegans Anillin proteins regulate intercellular bridge stability and germline syncytial organization

Rana Amini,[1] Eugénie Goupil,[1] Sara Labella,[3] Monique Zetka,[3] Amy S. Maddox,[1,2] Jean-Claude Labbé,[1,2] and Nicolas T. Chartier[1]

[1]Institute of Research in Immunology and Cancer and [2]Department of Pathology and Cell Biology, Université de Montréal, Montréal, Québec H3C 3J7, Canada
[3]Department of Biology, McGill University, Montréal, Québec H2A 1B1, Canada

Cytokinesis generally produces two separate daughter cells, but in some tissues daughter nuclei remain connected to a shared cytoplasm, or syncytium, through incomplete cytokinesis. How syncytia form remains poorly understood. We studied syncytial formation in the *Caenorhabditis elegans* germline, in which germ cells connect to a shared cytoplasm core (the rachis) via intercellular bridges. We found that syncytial architecture initiates early in larval development, and germ cells become progressively interconnected until adulthood. The short Anillin family scaffold protein ANI-2 is enriched at intercellular bridges from the onset of germ cell specification, and ANI-2 loss resulted in destabilization of intercellular bridges and germ cell multinucleation defects. These defects were partially rescued by depleting the canonical Anillin ANI-1 or blocking cytoplasmic streaming. ANI-2 is also required for elastic deformation of the gonad during ovulation. We propose that ANI-2 promotes germ cell syncytial organization and allows for compensation of the mechanical stress associated with oogenesis by conferring stability and elasticity to germ cell intercellular bridges.

Introduction

Cytokinesis, the last step of cell division, allows the physical separation of two daughter cells by abscission. Accordingly, it is precisely controlled, and cytokinetic failure can lead to aneuploidy, which can cause developmental alterations or have pathological consequences. Interestingly, during the development of certain tissues, some cells are programmed to undergo incomplete divisions to form a syncytium, wherein multiple nuclei remain connected by stable cytoplasmic intercellular bridges (Haglund et al., 2011; Lacroix and Maddox, 2012). For instance, in many species, including humans, germ cells are connected by intercellular bridges that were proposed to regulate germ cell development by facilitating nutrient sharing, and the absence of these bridges is associated with infertility (Brill et al., 2000; Greenbaum et al., 2006, 2011). Although many actin-associated proteins and cytokinetic regulators are enriched at intercellular bridges (Greenbaum et al., 2011; Haglund et al., 2011; Lacroix and Maddox, 2012), the mechanisms that regulate their timely formation, maintenance, and disassembly remain poorly understood.

The *Caenorhabditis elegans* germline comprises a powerful model system in which to study syncytial organization. Hermaphrodite adult animals possess two U-shaped gonad arms, each containing ~1,000 germ cells that are radially arranged around a central rachis, to which they are connected by an intercellular bridge (termed rachis bridge; Zhou et al., 2013), thus comprising a syncytium (Hirsh et al., 1976). Each gonad arm is organized in a polarized manner, from distal to proximal, such that germ cells at various stages of gametogenesis are physically segregated (see Fig. 3 A; Kimble and Crittenden, 2007). The most distal portion of the gonad contains ~200 mitotic germline stem cells. Germ cells that leave the distal region stop proliferating and begin meiotic differentiation, successively going through stages of meiotic prophase as they progress toward the proximal region. Differentiation culminates in the most proximal part of the gonad where oocyte growth is primarily sustained by an actin-dependent streaming of cytoplasm in the central rachis (Wolke et al., 2007; Kim

Correspondence to Nicolas T. Chartier: chartier.nico@gmail.com; or Jean-Claude Labbé: jc.labbe@umontreal.ca

A.S. Maddox's present address is Dept. of Biology, The University of North Carolina at Chapel Hill, 408 Fordham Hall, Chapel Hill, NC, 27599.

N.T. Chartier's present address is INSERM U823, Université Joseph Fourier-Grenoble 1, Institut Albert Bonniot, Grenoble F-38700, France.

Abbreviation used in this paper: NMY-2, nonmuscle myosin II.

© 2014 Amini et al. This article is distributed under the terms of an Attribution–Noncommercial–Share Alike–No Mirror Sites license for the first six months after the publication date (see http://www.rupress.org/terms). After six months it is available under a Creative Commons License (Attribution–Noncommercial–Share Alike 3.0 Unported license, as described at http://creativecommons.org/licenses/by-nc-sa/3.0/).

Supplemental material can be found at:
http://doi.org/10.1083/jcb.201310117

The Rockefeller University Press $30.00
J. Cell Biol. Vol. 206 No. 1 129–143
www.jcb.org/cgi/doi/10.1083/jcb.201310117

THE JOURNAL OF CELL BIOLOGY

Downloaded from jcb.rupress.org on July 9, 2017

et al., 2013). Mature oocytes lose their connection with the rachis and become cellularized, ready for ovulation and fertilization by sperm stored in the spermatheca (McCarter et al., 1999; Maddox et al., 2005). This structural organization ensures that oocytes are constantly produced in a conveyor belt–like fashion.

All germ cells in *C. elegans* originate from a common precursor (Wang and Seydoux, 2013). After fertilization, the zygote contains germline determinants and is referred to as the P_0 germline blastomere. During embryogenesis, germline determinants are progressively compartmentalized through four successive asymmetric divisions, resulting in the generation of a single germline blastomere termed P_4 (Fig. 1 A; Deppe et al., 1978). The P_4 blastomere divides symmetrically (at around the embryonic 100-cell stage) to give rise to the primordial germ cells Z_2 and Z_3, which do not undergo further division during the remainder of embryogenesis (Deppe et al., 1978; Sulston et al., 1983). As animals hatch in their first larval stage (L1) and begin to feed, Z_2 and Z_3 initiate proliferation and, through successive larval developmental stages (L2, L3, and L4), generate all germ cells in both gonad arms of the adult (Fig. 2 B; Hirsh et al., 1976).

Germline organization in *C. elegans* depends on a number of conserved actin-binding proteins that are enriched at the rachis bridge of germ cells (Maddox et al., 2005; Zhou et al., 2013). Among these proteins is ANI-2, a homologue of the actomyosin scaffold protein Anillin (Maddox et al., 2005). Whereas a canonical *C. elegans* Anillin homologue (termed ANI-1) is enriched in the cytokinetic furrow and predicted to bind nonmuscle myosin, F-actin, and septins (Field and Alberts, 1995; Oegema et al., 2000; Paoletti and Chang, 2000; Straight et al., 2005), ANI-2 is a shorter Anillin isoform that lacks the N-terminal domains predicted to bind myosin and actin, and was thus proposed to function as a competitive negative regulator of contractility (Chartier et al., 2011). ANI-2 decorates the surface of the rachis and is enriched at rachis bridges in adult hermaphrodites (Maddox et al., 2005). In the proximal gonad, gametes progressively cellularize and detach from the rachis, so that mature oocytes and fertilized embryos contain very little ANI-2 protein (Maddox et al., 2005; Chartier et al., 2011). Partial depletion of ANI-2 by RNAi causes precocious oocyte cellularization, whereas more thorough depletion results in severe germline disorganization, germ cell multinucleation, and adult sterility (Maddox et al., 2005; Green et al., 2011).

How the syncytial architecture of the *C. elegans* germline arises during development is unknown. Here, we present the first characterization of the genesis and topology of gonad syncytial architecture throughout development. We find that ANI-2 is expressed early in germline development and is required for the stabilization of the intercellular bridges that connect germ cells to the rachis, in part by opposing ANI-1 activity. Loss of ANI-2 leads to germ cell multinucleation, which can be rescued by blocking cytoplasmic streaming in the rachis. Our results support a model in which ANI-2 stabilizes intercellular bridges and makes them robust to mechanical stress at the onset of oogenesis.

Results

ANI-2 is enriched at the rachis bridge of all germ cells throughout gonad development

To address how the germline syncytium is formed and maintained, we first sought to identify a marker that would enable the monitoring of syncytial organization throughout development. As ANI-2 was previously reported to localize to the rachis of adult animals (Maddox et al., 2005), we analyzed its spatiotemporal localization throughout *C. elegans* development. In wild-type embryos, endogenous ANI-2 was present in very low amounts throughout early embryogenesis, as previously reported (Chartier et al., 2011), but appeared specifically in the P_4 germline blastomere (Fig. 1 B). ANI-2 accumulated at the cell equator during cytokinesis as P_4 divided to produce Z_2 and Z_3, and remained enriched at the midbody that was formed between the two primordial germ cells (Fig. 1, C and D). The timing of *ani-2* expression is similar to that reported for many germline-specific genes that are controlled by the transcriptional repressor PIE-1 (Wang and Seydoux, 2013). We perturbed germline specification by depleting PIE-1 and found that ANI-2 was undetectable in these embryos (Fig. 1 E). In contrast, when we depleted MEP-1 to deregulate germline gene expression, ANI-2 was present in multiple cells (Fig. 1 E). This indicates that ANI-2 is a bona fide germline-enriched protein that is expressed early during germ cell specification and stably accumulates between the two primordial germ cells.

We next monitored ANI-2 distribution throughout germline development in animals coexpressing ANI-2 fused to GFP (GFP::ANI-2) and a membrane marker, an mCherry-tagged probe previously shown to decorate the plasma membrane (Kachur et al., 2008; Green et al., 2011). Similar to endogenous ANI-2 (Maddox et al., 2005), GFP::ANI-2 localized between Z_2 and Z_3 in newly hatched L1 larvae and was present in all germ cells during larval development and into adulthood (except in the most mature oocytes), lining the rachis and becoming progressively enriched at rachis bridges (Fig. 2 A). These results indicate that ANI-2 is present in all germ cells and enriched at rachis bridges throughout germline development, from the birth of primordial germ cells to the completion of oocyte maturation, making it an ideally suited marker to monitor syncytium organization during development.

The syncytial architecture of the *C. elegans* gonad arises progressively during larval development

To determine how the syncytial architecture of the germline arises during development, we developed a fluorescence microscopy–based assay to monitor the organization of rachis bridges. We measured the cortical fluorescence intensity in multiple optical sections of germ cells coexpressing GFP::ANI-2 and the membrane marker (Fig. 3 B). A given germ cell was considered to be open to the rachis when a minimum in membrane marker fluorescence intensity was detected between two distinct fluorescence intensity peaks of GFP::ANI-2 (Fig. 3, C and D; see Materials and methods). Rachis bridge diameter was assessed by measuring the distance between the peaks of intensity for

Downloaded from jcb.rupress.org on July 9, 2017

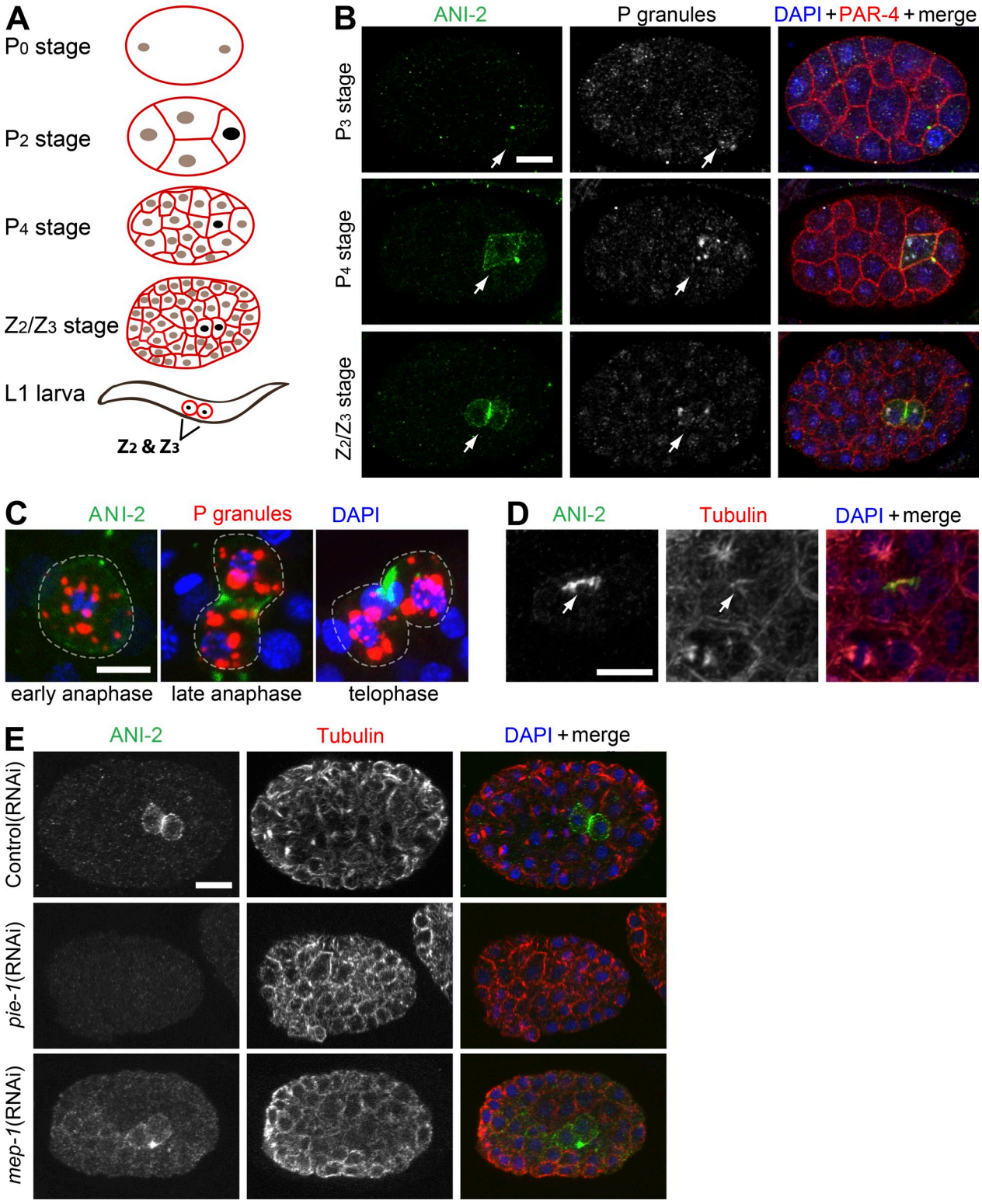

Figure 1. **ANI-2 stably accumulates at the midbody between the two primordial germ cells.** (A) Schematic representation of germ cell specification (black nuclei) during embryonic development. The primordial germ cells Z_2 and Z_3 are born from the P_4 blastomere and do not undergo further division until hatching. (B) Mid-section confocal images of fixed wild-type embryos immunostained with ANI-2 (green), P-granules (PGL-1, gray), PAR-4 (to label the cortex, red), and DAPI (blue). Arrows point to the germline blastomeres. Bar, 10 µm. (C) Confocal projections of the dividing P_4 blastomere in fixed wild-type embryos immunostained with ANI-2 (green), P-granules (PGL-1, red), and DAPI (blue). The white dashed line delineates the cell membrane. Bar, 5 µm. (D) Mid-section confocal images of the primordial germ cells of a fixed wild-type embryo immunostained with ANI-2 (green), α-tubulin (red), and DAPI (blue). Arrows point to the midbody. Bar, 5 µm. (E) Mid-section confocal images of fixed wild-type (top), *pie-1(RNAi)* (middle), and *mep-1(RNAi)* (bottom) embryos immunostained with ANI-2 (green), α-tubulin (red), and DAPI (blue). In all frames, anterior is to the left. Bar, 10 µm.

Downloaded from jcb.rupress.org on July 9, 2017

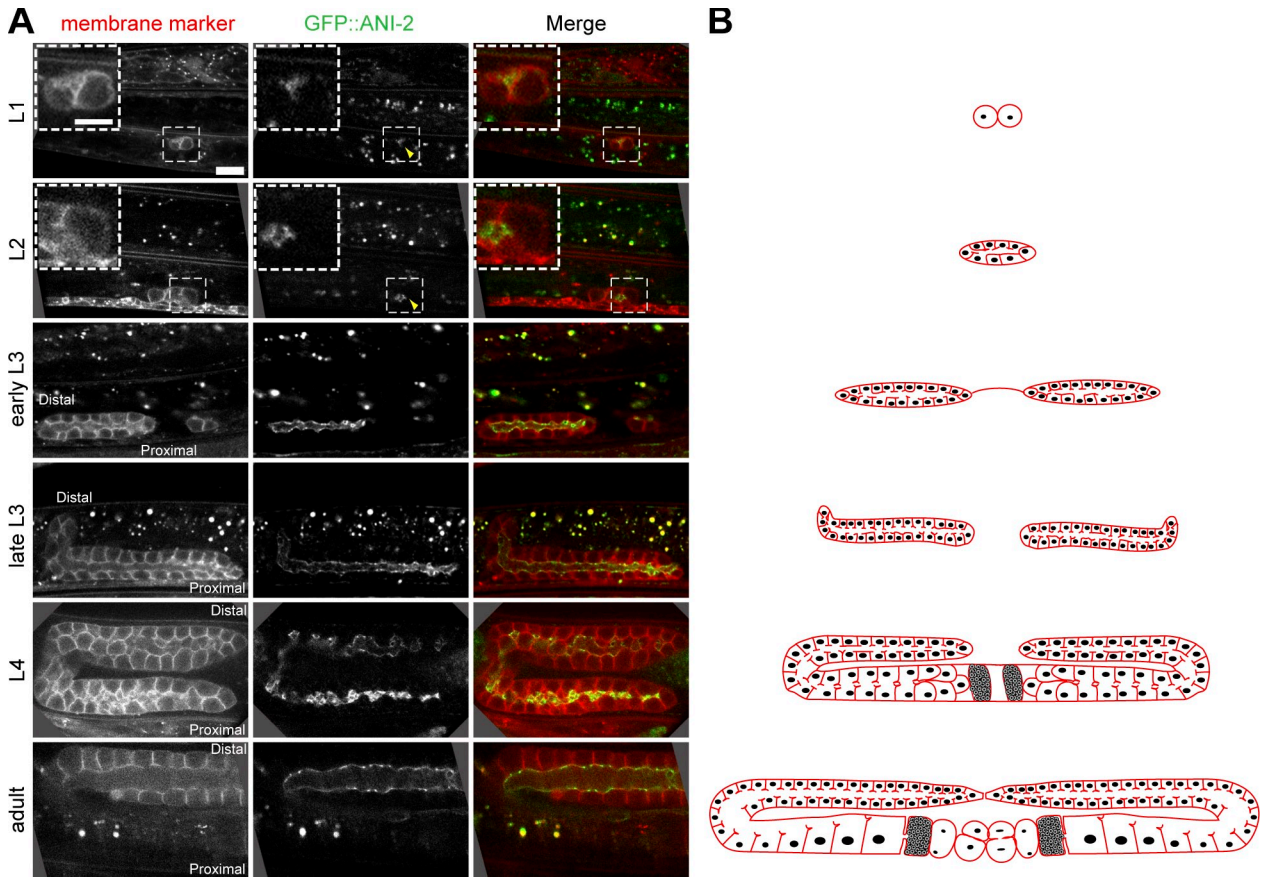

Figure 2. **ANI-2 is found at the rachis bridge of all germ cells throughout larval development.** (A) Mid-section confocal images of the germline of wild-type hermaphrodites expressing GFP::ANI-2 (green, yellow arrowheads) and a membrane marker (red) at various stages of development. For simplicity, only one gonad arm is shown from the L3 stage onward. In all frames, anterior is to the left. Bar, 10 µm. The regions delineated by the white dashed squares are magnified in the inset (bar for insets, 5 µm). (B) Schematic representation of germline development at the developmental stages shown in E. Germ cells undergo proliferation and differentiation during larval growth until animals reach adulthood. For simplicity, only the germline is depicted.

each marker, and bridges were considered to be open when their diameter was >0.8 µm.

We first applied this assay to the germ cells of adult animals, as germline syncytial organization is well described for this developmental stage (Hirsh et al., 1976; Hall et al., 1999). All germ cells examined (28/28), including the most distal cells, had a characteristic minimum in membrane marker intensity between two peaks of GFP::ANI-2 intensity (Fig. 3 G), indicating, as expected, that all cells have an open (>0.8 µm) connection to the rachis at this stage.

Analysis of rachis bridge organization during larval development revealed that many germ cells are also open to the rachis at the L4 stage (128/130), late L3 stage (96/117), early L3 stage (71/106), and L2 stage (29/53; Fig. 3 G). However, for other germ cells at these larval stages, only a single peak of GFP::ANI-2 intensity was detected (Fig. 3, E and F), suggesting that these germ cells are not connected to the central rachis through an open bridge. The proportion of germ cells with this latter GFP::ANI-2 distribution was highest in L2 animals, decreased progressively throughout larval development, and was zero in adult animals (Fig. 3 G). Moreover, we observed that rachis bridge diameter (when open) increased gradually as animals progressed through larval development (Fig. 3 H). Similar results were obtained when we measured rachis bridge organization in animals expressing GFP-tagged versions of the canonical Anillin ANI-1 or nonmuscle myosin II (NMY-2), two contractility regulators that, like ANI-2, accumulate at germ cell rachis bridges (Fig. S1; Nance et al., 2003; Maddox et al., 2007). These results indicate that germline syncytial organization occurs progressively during larval development.

We next applied this assay to test whether primordial germ cells in newly hatched L1 larvae are interconnected. According to the localization pattern of GFP::ANI-2 and the membrane marker, Z_2 and Z_3 did not appear to share a cytoplasmic connection (5/5; Fig. 3 G). However, we reasoned that the small measurable zone between these germ cells could confound the fluorescence intensity assay. To independently verify that these cells indeed lacked a cytoplasmic connection, we monitored the diffusion of cytoplasmic, exogenously supplied photo-convertible rhodamine-dextran in the primordial germ cells Z_2 and Z_3. Whereas photoactivation of rhodamine-dextran resulted in its rapid diffusion within a single germ cell (Fig. S2; see also Green et al., 2013), we did not detect significant fluorescence accumulation in the sister germ cell up to 30 min after photoactivation (Fig. 3, I and J). Together, these results indicate that the two primordial germ cells Z_2 and Z_3 are linked by an intercellular bridge that has

Downloaded from jcb.rupress.org on July 9, 2017

a small diameter and allows little or no cytoplasmic exchange, and that rachis bridge opening occurs progressively during larval development, culminating at the adult stage in a germline that is fully syncytial.

ANI-2 is required for rachis bridge stability

ANI-2 is found in all germ cells of larvae and adult animals (except for the cellularized oocytes), suggesting that it regulates rachis bridge formation and/or maintenance. To test this possibility, we measured rachis bridge organization in the germline of living *ani-2(ok1147)* mutant animals coexpressing the fluorescent membrane marker and GFP::ANI-1. *ok1147* is a presumptive null allele of *ani-2*, and homozygous mutant embryos develop into sterile adult animals with a very disorganized germline containing multinucleated, abnormally sized germ cells, similar to the phenotype reported after ANI-2 depletion by RNAi (see the following section and Fig. 5 A; Green et al., 2011). Surprisingly, however, the germline morphology of *ani-2* mutant L4-stage larvae was largely normal, with regularly sized and spaced mononucleated germ cells lining the gonad wall (Fig. 4, A and C). Despite these aspects of morphology being normal, rachis bridge organization in *ani-2* mutant L4 stage animals was abnormal. Whereas nearly all control germ cells had open rachis bridges (i.e., >0.8 µm; Fig. 4, B and E), the majority of germ cells (46/68) in L4-stage *ani-2* mutant animals lacked a defined opening to the rachis and a single peak of GFP::ANI-1 intensity was detected (Fig. 4, D and E). In the minority of germ cells in which an open rachis bridge was detected (22/68), the diameter of the bridge was significantly smaller than that measured in control animals (Fig. 4 F). Rachis bridges were also largely absent from the germ cells of younger larvae (early L3; Fig. 4 E). Similar results were obtained from strains coexpressing the membrane marker with either NMY-2::GFP or GFP::PGL-1, a germline P granule component that decorates the surface of germ cell nuclei (Kawasaki et al., 1998; Merritt et al., 2008; Fig. S3). We conclude that ANI-2 is required for the formation and/or maintenance of germ cell rachis bridges during germline development.

ANI-2 stabilizes the membrane partitions between germ cells from the late L4 larval stage

Animals lacking ANI-2 fail to form rachis bridges during larval development and become sterile adults with multinucleated germ cells (Fig. 5 A), suggesting that multinucleation is a consequence of defects in rachis bridge formation. To address this possibility, we monitored germline development in animals coexpressing the membrane marker fused to GFP and histone H2B fused to mCherry (Green et al., 2011). We found that until *ani-2* mutant animals reached the L4 larval stage, germline expansion proceeded largely normally; the number of germ cells was comparable to that of control animals at all stages and most germ cells contained a single nucleus (Fig. 5 A). In addition, immunofluorescence analysis of gonads from young adult animals revealed that the germ cells of *ani-2* mutants can enter meiotic differentiation and form sperm, although male mating assays revealed that the sperm are not functional (Fig. S4 A; unpublished data). The primary defect of *ani-2* mutant gonads during early larval development was a marked decrease in rachis diameter (Fig. S4 B). Thus, cell proliferation and entry into meiosis are not grossly impaired in *ani-2* mutants and germline development is largely normal during early larval stages.

In contrast, in the proximal gonad of late L4-stage *ani-2* mutant animals, abnormal multinucleated germ cells were present, albeit at low frequency (Fig. 5, A and B). In young adult animals, multinucleated germ cells increased in proportion, and were observed in progressively more distal regions of the gonad (Fig. 5, A and B). In the gonads of older adult *ani-2* mutant animals (20–48 h post-L4), most germ cells were multinucleated and the number of nuclei per compartment was higher than in previous developmental stages (Fig. 5 C). Furthermore, the germ cells of *ani-2* mutant animals did not complete meiosis and showed a defect in diakinesis (Fig. S4 A). Multinucleation and diakinesis defects were never observed in the gonads of control animals ($n > 100$). Loss of ANI-2 therefore results in abnormal germ cell multinucleation, initially in the proximal gonad region of late L4 stage animals but progressively affecting the entire germline.

Multinucleation, together with the abnormal execution of diakinesis, is likely key to the sterility of *ani-2* mutant animals. Multinucleation could arise from cumulative cytokinetic failures of dividing germline stem cells in the distal region of the gonad. However, time-lapse analysis of germline stem cell division in *ani-2* mutants revealed that they undergo normal cytokinesis (Fig. S4 D). Likewise, multinucleation did not arise from germ cells abnormally reentering mitosis, as depletion of the mitotic regulators CDK-1 or PLK-1 by RNAi did not prevent this defect (Fig. S4 E; unpublished data). These results indicate that the multinucleation defect of *ani-2* mutant germ cells is not a consequence of inappropriate cell division.

Because ANI-2 localizes to rachis bridges in wild-type animals, we considered the possibility that multinucleation in *ani-2* mutants arises from a collapse of membrane partitions between germ cells. Time-lapse analysis of the proximal gonad of late L4-stage and young adult *ani-2* mutants revealed two clearly defined instances of germ cell partition collapse, resulting in multinucleation (Fig. 5 D). This is likely an underestimation of the frequency of this defect, as our experimental imaging conditions may have masked several more of these events (see Materials and methods). Together with our finding that germ cells do not enter mitosis inappropriately, these results indicate that ANI-2 is required starting at the L4 larval stage to maintain proper organization of the germline, at least in part by preventing the collapse of germ cell partitions.

ANI-2 and ANI-1 have opposing activities in germline organization

ANI-2 was previously proposed to regulate contractility by competing with the canonical Anillin ANI-1 for one or more contractility regulators (Chartier et al., 2011), suggesting that the defects observed in *ani-2* mutants may result from ANI-1 hyperactivation. To test this, we first characterized the phenotype of *ani-1(RNAi)* animals coexpressing GFP::ANI-2 and the membrane marker (Fig. 6 A). We found that depleting ANI-1

Downloaded from jcb.rupress.org on July 9, 2017

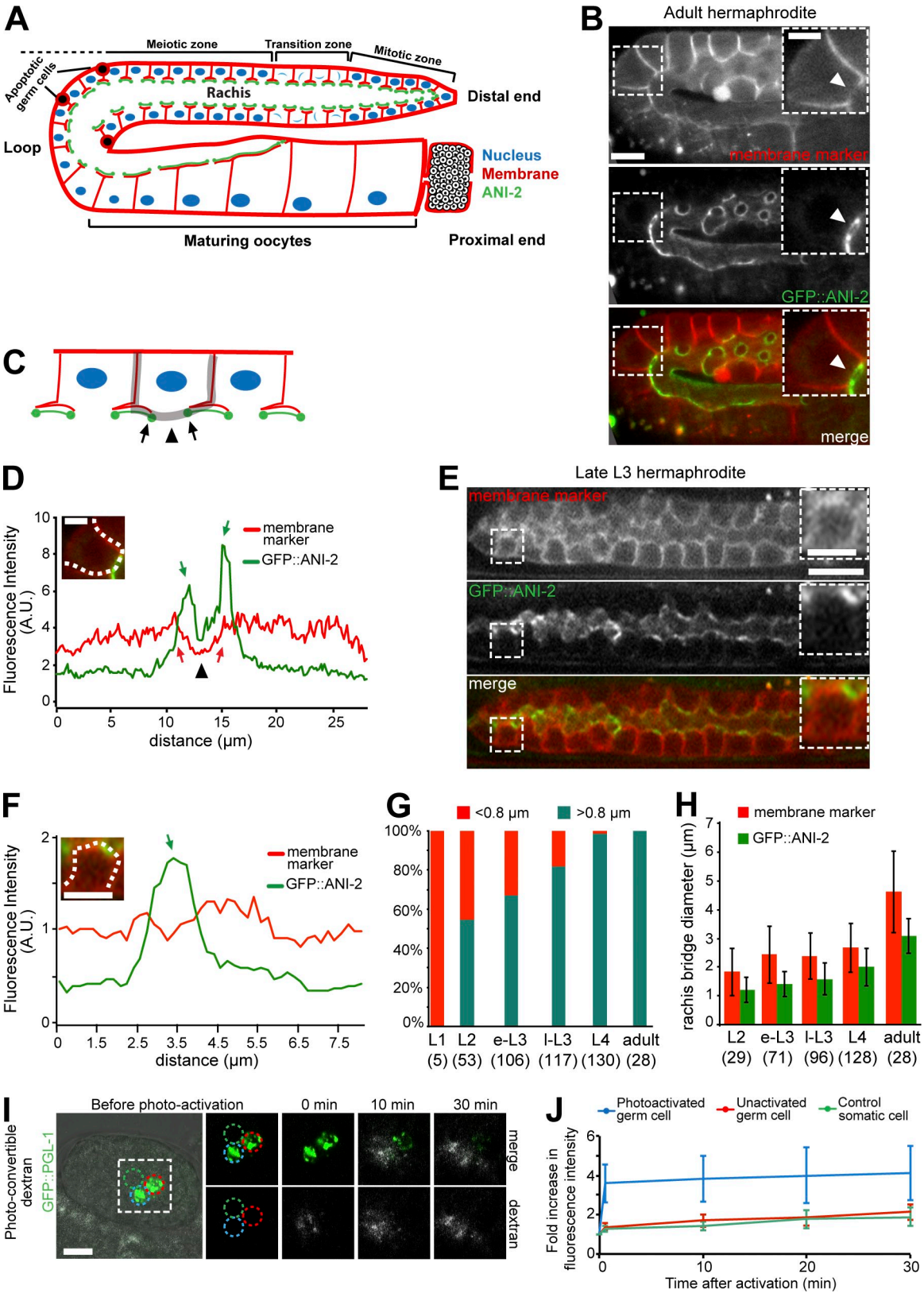

Figure 3. **Germ cell rachis bridge formation arises progressively during larval development.** (A) Schematic representation of the adult hermaphrodite germline. ANI-2 (green) lines up at the periphery of the central rachis and is enriched at rachis bridges, and it is delocalized upon oocyte cellularization. (B and E) Mid-section confocal images of the germline of a wild-type adult (B) and L3 (E) hermaphrodites expressing GFP::ANI-2 (green) and a membrane marker (red). Bar, 10 µm. The regions delineated by the white dashed square are magnified in the inset (bar for insets, 5 µm). In B, the white arrowhead points to the germ cell opening to the rachis. (C) Schematic representation of germ cells as in A depicting the method for measuring rachis bridge organization. Fluorescence intensity is measured along the lateral and apical cortices (line shown in black). Arrows point to the position of the rachis bridge as seen in mid-section images, and the arrowhead points to the germ cell opening to the rachis. (D and F) Measured fluorescence intensities (in arbitrary

Downloaded from jcb.rupress.org on July 9, 2017

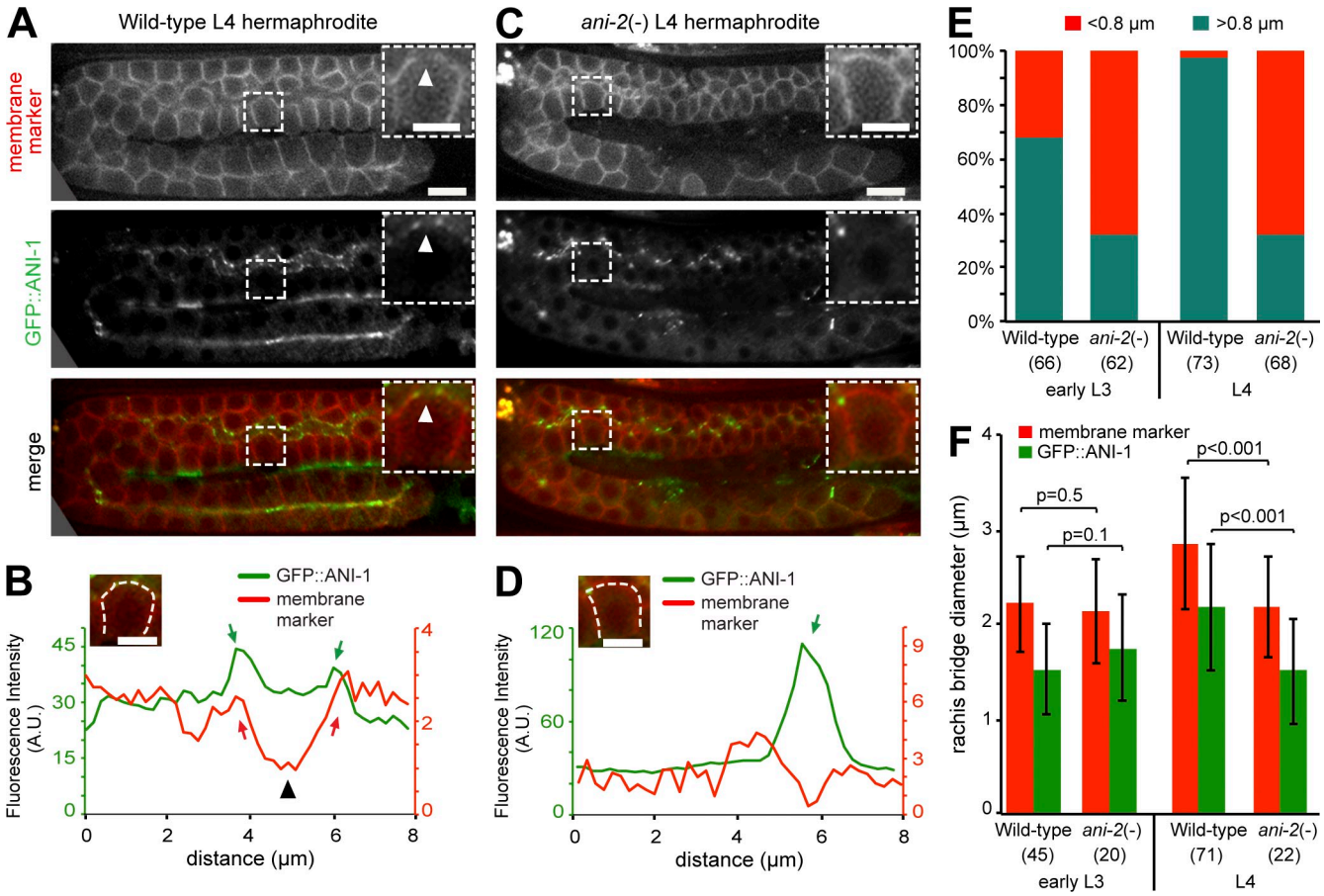

Figure 4. **ANI-2 is required for rachis bridge stabilization.** (A and C) Mid-section confocal images of the germline of a wild-type (A) and an *ani-2*(−) (C) L4 hermaphrodite expressing a membrane marker (red) and GFP::ANI-1 (green). Bar, 10 µm. The regions delineated by the white dashed square are magnified in the inset (bar for insets, 5 µm). In A, the white arrowhead points to the germ cell opening to the rachis. (B and D) Measured fluorescence intensities (in arbitrary units specific to each curve) for each fluorescent marker along the lateral and apical cortices (white dotted line, as shown in insets; bar for insets, 5 µm) of the germ cell magnified in A and C, respectively. Red and green arrows point to peaks of membrane marker and GFP::ANI-1 fluorescence intensities, respectively, and the black arrowhead points to the intensity minimum. (E) Proportion of germ cells showing rachis bridges with a diameter >0.8 µm (turquoise) or <0.8 µm (red) in wild-type and *ani-2*(−) mutant animals at the L3 and L4 larval stages, as measured by fluorescent marker distribution. (F) Maximal rachis bridge diameter in germ cells of wild-type and *ani-2*(−) animals at the L3 and L4 larval stages, as measured with membrane (red) or GFP::ANI-1 (green) fluorescence distribution. Rachis bridges that are <0.8 µm in diameter are excluded from this analysis. Error bars represent SD. In E and F the numbers in brackets represent the total number of germ cells analyzed.

by RNAi did not cause prominent gonad disorganization in adult hermaphrodites and that all germ cells had an intercellular bridge open to the rachis (Fig. 6 B). However, we observed several defects that were opposite to those observed in *ani-2* mutants. In *ani-1(RNAi)* animals, the diameter of rachis bridges was larger and the diameter of the rachis was increased as compared with the control (Fig. 6 C and Fig. S4 C). Additionally, oocyte cellularization was delayed (Fig. 6 A; unpublished data). Animals depleted of ANI-1 also showed a number of other defects not observed in *ani-2* mutants, such as a low frequency of bi-nucleated cells (unpublished data), consistent with ANI-1's function in regulating cytokinesis. These results indicate that ANI-1 is active in the germline and that its depletion results in defects opposite to those of *ani-2* mutants.

We next asked if the phenotypes observed in the gonad of *ani-2* mutants are a consequence of increased ANI-1 activity. To test this, we measured germline organization in *ani-2* mutant animals in which ANI-1 was depleted by RNAi (Fig. 6 D).

units) for each fluorescent marker along the lateral and apical cortices (white dotted line, as shown in insets; bar for insets, 5 µm) of the germ cell magnified in B and E, respectively. Red and green arrows point to peaks of membrane marker and GFP::ANI-2 fluorescence intensities, respectively. Both peaks border a minimum in fluorescence intensity (black arrowhead) that corresponds to the germ cell opening to the rachis. (G) Proportion of germ cells showing rachis bridges with a diameter >0.8 µm (turquoise) or <0.8 µm (red) throughout larval development, as measured by fluorescent marker distribution. (H) Maximal rachis bridge diameter in germ cells throughout larval development, as measured with GFP::ANI-2 (green) or membrane (red) fluorescence distribution. Error bars represent SD. In G and H the numbers in brackets represent the total number of germ cells analyzed. (I) Mid-section confocal images of an embryo expressing GFP::PGL-1 (green) exogenously supplied with photo-convertible rhodamine-dextran (gray). Time is relative to fluorescence photoactivation (at time 0) in one of the two primordial germ cells (blue dashed circle). The sister cell is delineated by a red dashed circle and the green dashed circle delineates a nearby somatic cell. Bar, 10 µm. (J) Fold-increase (from time 0) in fluorescence intensity over time measured in each cell shown in I. Error bars represent SD over 13 embryos.

Downloaded from jcb.rupress.org on July 9, 2017

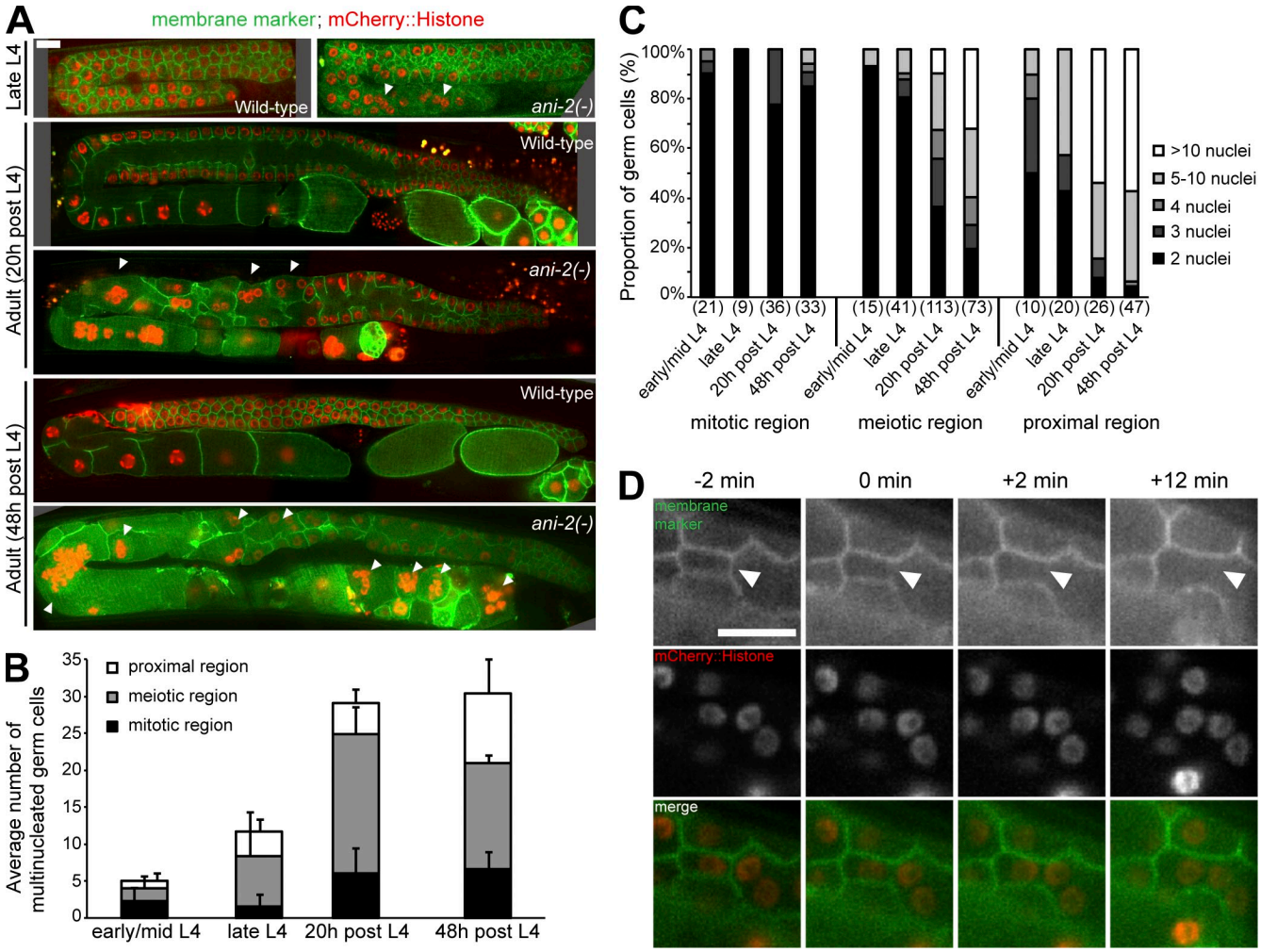

Figure 5. **Loss of ANI-2 causes germ cell multinucleation and collapse of membrane partitions.** (A) Mid-section confocal images of the germline of wild-type and *ani-2*(−) hermaphrodite animals at various stages of development expressing a membrane marker (green) and mCherry::Histone H2B (red). Each image was assembled from multiple acquisitions of the same animal. Arrowheads point to multinucleated germ cells. (B) Average number of multinucleated germ cells in various germline regions of *ani-2*(−) mutant hermaphrodites at the specified stage. Multinucleation was never observed in control animals at any stage. Error bars represent SD over 5–9 animals at each stage. (C) Proportion of multinucleated germ cells with 2, 3, 4, 5–10, and >10 nuclei in various germline regions of *ani-2*(−) hermaphrodites at the specified stage. The number of germ cells analyzed is shown for each condition. (D) Mid-section confocal time-lapse images of germ cells of an *ani-2*(−) hermaphrodite expressing a membrane marker (green) and mCherry::Histone H2B (red) captured during the collapse of a membrane partition (arrowhead). The stages examined and reported are early-mid L4 larvae, late L4 larvae, 20 h post-L4 stage, and 48 h post-L4 stage. Bars (A and D), 10 µm.

Whereas the germline of these *ani-2*(−); *ani-1(RNAi)* animals remained severely disorganized, we found that several *ani-2*–related defects were slightly but significantly rescued. As compared with control *ani-2* mutant L4 hermaphrodites, we found that depleting ANI-1 resulted in an increase in the number of germ cells that were open to the rachis and an increase in rachis bridge diameter (Fig. 6, E and F). Furthermore, whereas the number of multinucleated germ cells was not different from control, we measured a significant decrease in the number of nuclei per multinucleated compartment in the proximal and meiotic regions of young adult hermaphrodite gonads (20 h post-L4; Fig. 6, G and H). Altogether, these results indicate that the defects observed in *ani-2* mutants are partly due to an increase in ANI-1 activity and that proper germline organization and function requires a balance between the activity of these two Anillin proteins.

Cytoplasmic streaming in the rachis contributes to germline disorganization in *ani-2* mutants

Germ cell multinucleation in *ani-2* mutants is first observed in late L4-stage animals, near the time when the proximal-most germ cells begin to grow and mature as oocytes. Oocyte growth results largely from an actin-dependent distal-to-proximal movement of cytoplasm in the rachis, which initiates as animals enter adulthood (Wolke et al., 2007; Kim et al., 2013). We reasoned that cytoplasmic streaming could cause mechanical stress in the gonad and lead to a collapse of germ cell partitions and germline multinucleation in gonads lacking full ANI-2 function. To test this hypothesis, we first determined whether cytoplasmic streaming occurs in the rachis of *ani-2* mutant animals. We found that streaming initiates properly in the gonads of *ani-2* mutant hermaphrodites (Fig. 7, A and B), although velocity is

Downloaded from jcb.rupress.org on July 9, 2017

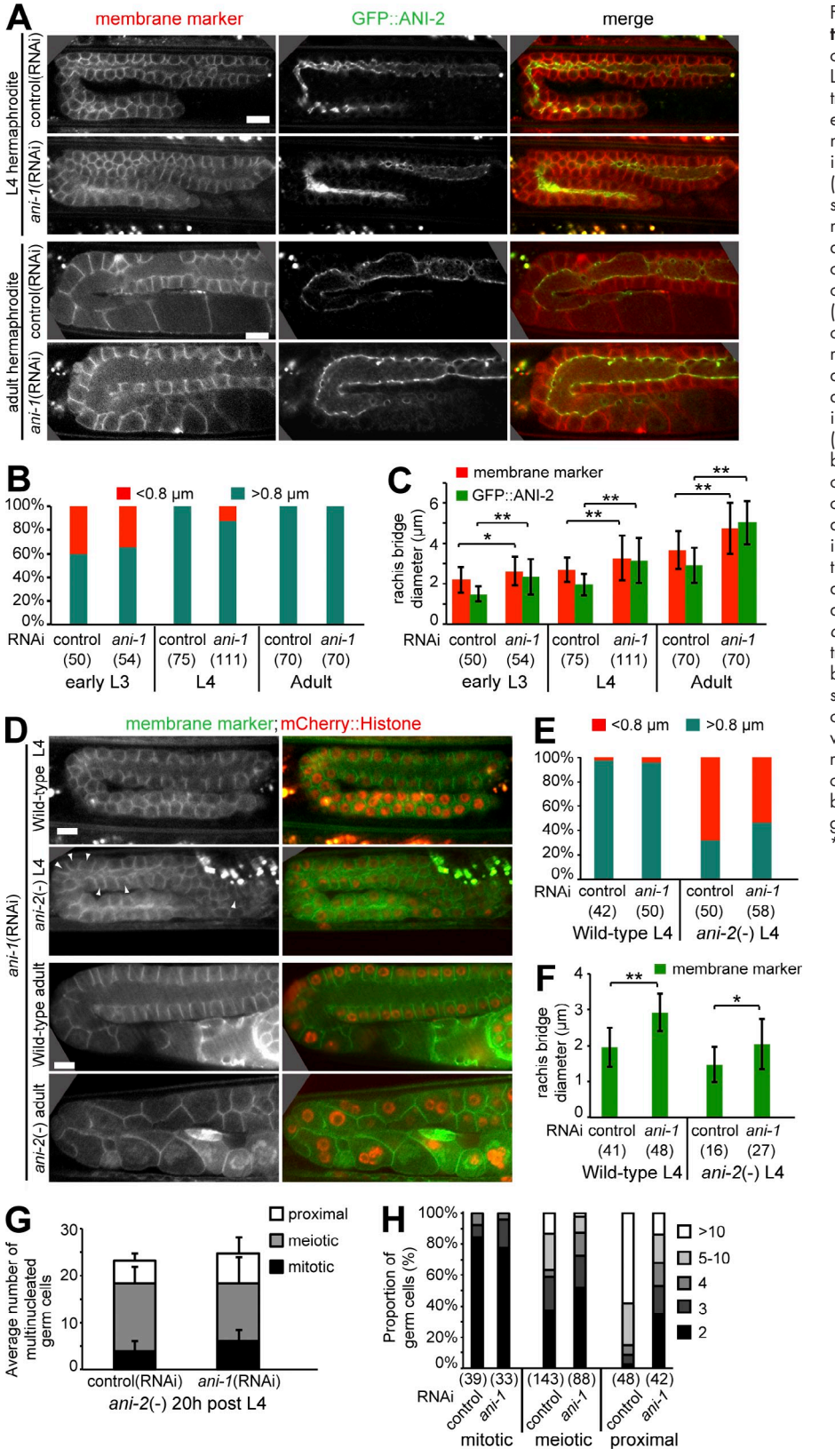

Figure 6. **ANI-2 and ANI-1 have opposing activities in germline organization.** (A) Mid-section confocal images of the germline of wild-type L4 (top) and adult (bottom) hermaphrodites, treated with control(RNAi) or *ani-1(RNAi)*, and expressing GFP::ANI-2 (green) and a membrane marker (red). (B) Proportion of germ cells showing rachis bridges with a diameter >0.8 µm (turquoise) or <0.8 µm (red) in animals of the specified condition, as measured by fluorescent marker distribution. (C) Maximal rachis bridge diameter in germ cells of animals of the specified condition, as measured with membrane (red) or GFP::ANI-2 (green) fluorescent distribution. (D) Mid-section confocal images of the germline of wild-type and *ani-2*(−) young adult hermaphrodites (20 h post-L4), treated with *ani-1(RNAi)*, and expressing a membrane marker (green) and mCherry::Histone H2B (red). Arrowheads indicate germ cells with open rachis bridges. (E) Proportion of germ cells showing rachis bridges with a diameter >0.8 µm (turquoise) or <0.8 µm (red) in animals of the specified condition, as measured by fluorescent marker distribution. (F) Maximal rachis bridge diameter in germ cells of animals of the specified condition, as measured with membrane fluorescent distribution. (G) Average number of multinucleated germ cells in various germline regions of *ani-2*(−) mutant hermaphrodites (20 h post-L4) treated with control(RNAi) or *ani-1(RNAi)*. Error bars represent SD over 10–17 animals at each stage. (H) Proportion of multinucleated germ cells with 2, 3, 4, 5–10, and >10 nuclei in various germline regions of *ani-2*(−) hermaphrodites (20 h post-L4) treated with control(RNAi) or *ani-1(RNAi)*. In B, C, E, F, and H, the numbers in brackets represent the total number of germ cells analyzed. Bars, 10 µm. *, $P < 0.01$; **, $P < 0.001$.

slightly reduced compared with wild-type adult animals (Fig. 7 C). In addition, whereas streaming is unidirectional toward the proximal end of the gonad in wild-type animals, the trajectory of cytoplasmic streaming in *ani-2* mutants was variable (Fig. 7 B). This indicates that cytoplasmic streaming, although disorganized, initiates properly in the gonads of *ani-2* mutants.

We then tested whether ANI-2 is required to stabilize the membrane partitions between germ cells and prevent

Downloaded from jcb.rupress.org on July 9, 2017

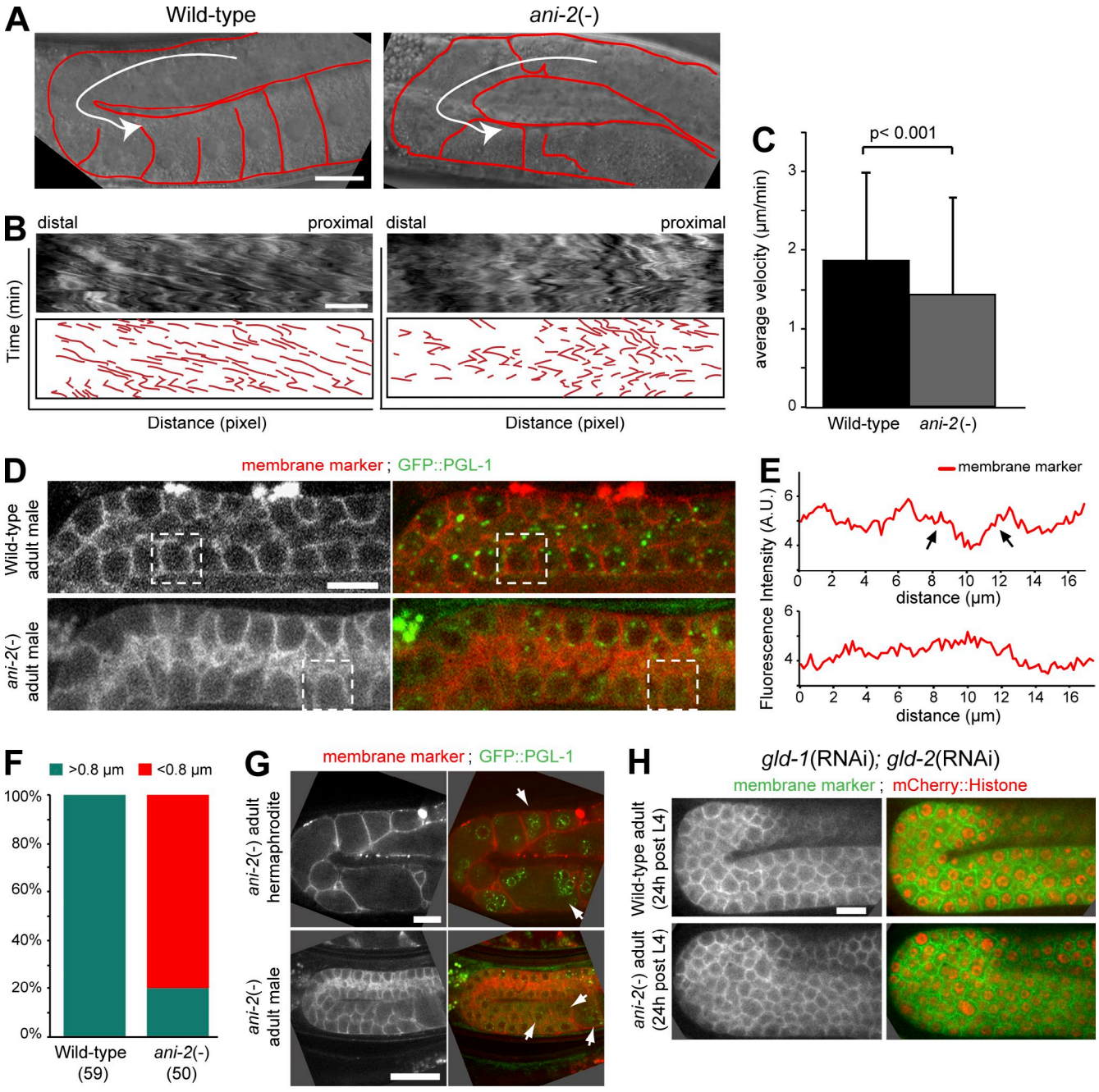

Figure 7. **Cytoplasmic streaming in the rachis may be responsible for germline disorganization in *ani-2* mutants.** (A) DIC images of the germlines of wild-type (left) and *ani-2*(−) (right) young adult animals. Some membrane partitions are outlined in red. The white arrow depicts the direction of cytoplasmic streaming. (B) DIC images (top) and schematic representations (bottom) of kymographs of cytoplasmic streaming in the gonads of animals depicted in A. Kymographs were made along the white line shown in A. The total duration of the movie is 45 min. (C) Average velocity of cytoplasmic streaming in the rachis of wild-type (black) and *ani-2*(−) (gray) animals. Error bars represent SD over 9 animals analyzed for each genotype. (D) Mid-section confocal images of a wild-type (top) and an *ani-2*(−) (bottom) male adult germline expressing a membrane marker (red) and GFP::PGL-1 (green). (E) Measured fluorescence intensities (in arbitrary units) for the membrane marker along the lateral and apical cortices of the germ cells of each male genetic background delineated by a dashed square in D. Arrows point to peaks of membrane marker fluorescence intensity bordering a minimum. (F) Proportion of germ cells showing rachis bridges with a diameter >0.8 μm (turquoise) or <0.8 μm (red) in wild-type and *ani-2*(−) animals at the adult stage, as measured by membrane marker distribution. The numbers in brackets represent the total number of germ cells analyzed. (G) Mid-section confocal images of the germlines of an *ani-2*(−) adult hermaphrodite (top) and an *ani-2*(−) adult male (bottom) expressing a membrane marker (red) and GFP::PGL-1 (green). Arrows point to multinucleated germ cells, whose number is significantly reduced in *ani-2*(−) males. (H) Mid-section confocal images of the gonads of wild-type (top) and *ani-2*(−) (bottom) adult hermaphrodites expressing a membrane marker (green) and mCherry::Histone H2B (red) and depleted of GLD-1 and GLD-2 by RNAi. Bars, 10 μm.

Downloaded from jcb.rupress.org on July 9, 2017

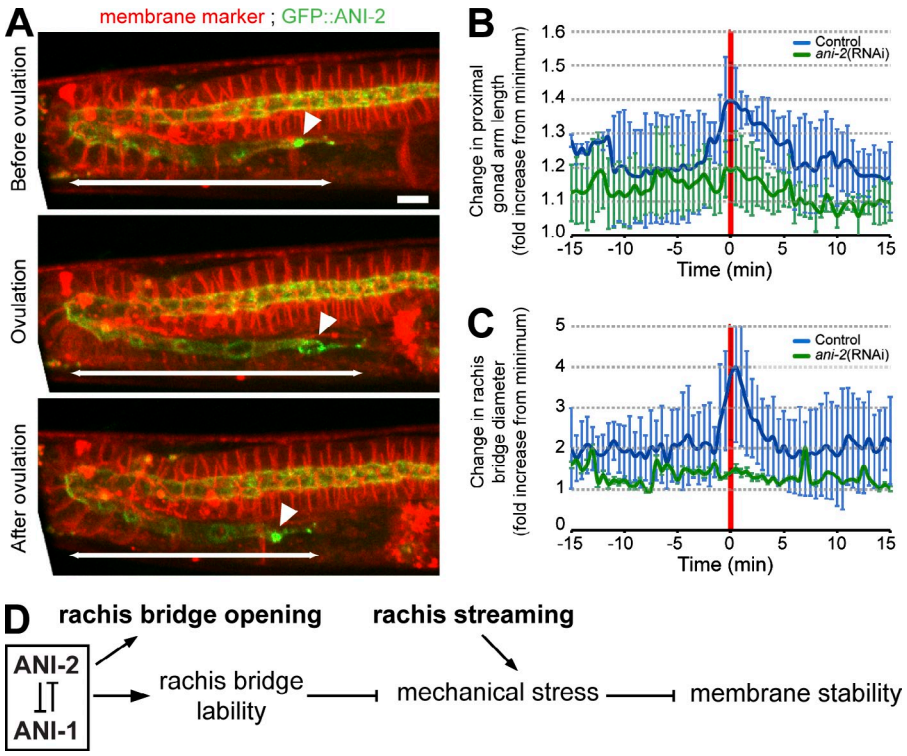

Figure 8. **ANI-2 permits elastic deformation of the adult hermaphrodite gonad and rachis bridges.** (A) Time-lapse confocal image projections of the gonad of a wild-type hermaphrodite expressing GFP::ANI-2 (green) and a membrane marker (red) captured before (top), during (middle), and after (bottom) ovulation. Arrowheads point to the most proximal rachis bridge. Double-headed arrows indicate the length of the GFP::ANI-2–enriched portion of the proximal gonad arm. Bar, 10 µm. See also Videos 1 and 2. (B and C) Measured fold-increase (as compared with minimum measurement) in proximal gonad arm length (B) and rachis bridge diameter (C) over time in the gonads of control (blue, *n* = 6) and *ani-2(RNAi)* (green, *n* = 5) adult hermaphrodite animals undergoing ovulation. Time 0 corresponds to the point of oocyte entry into the spermatheca. Error bars represent SD. (D) Proposed model depicting ANI-1 and ANI-2 function in promoting rachis bridge opening during larval development and relieving mechanical stress upon oogenesis in adult animals.

multinucleation in the absence of cytoplasmic streaming. We first tested this by examining the gonads of male animals, which are naturally devoid of cytoplasmic streaming (Wolke et al., 2007). Similar to the germ cells of adult hermaphrodites, we confirmed that the germ cells of adult wild-type males form rachis bridges and that ANI-2 is required for the maintenance of these bridges (Fig. 7, D–F). However, unlike in *ani-2* mutant hermaphrodites, the germ cells in *ani-2* mutant males were largely mononucleated (Fig. 7 G). We also inhibited streaming in the rachis of *ani-2* mutant hermaphrodites by depleting GLD-1 and GLD-2, which blocks germ cells from entering meiosis and results in a germline devoid of gametes, filled with mitotically competent cells (Francis et al., 1995). We found that both the number of multinucleated germ cells and the number of nuclei per multinucleated compartment were significantly lower in adult *ani-2* mutant hermaphrodites depleted in GLD-1 and GLD-2 compared with control *ani-2* mutant animals (Fig. 7 H). Similar results were obtained using *gld-1*(−); *gld-2*(−); *ani-2*(−) triple mutant animals (unpublished data). Thus, the absence of cytoplasmic streaming largely rescues the multinucleation phenotype observed in *ani-2* mutant germlines. Together, these results support the notion that the collapse of germ cell partitions and multinucleation of *ani-2* mutant germlines is caused by cytoplasmic streaming in the rachis.

ANI-2 permits elastic deformation of the adult hermaphrodite gonad and rachis bridges

Our results support a model in which ANI-2 stabilizes rachis bridges and prevents collapse of germ cell partitions by counterbalancing the mechanical stress caused by cytoplasmic streaming in the rachis. ANI-2 could compensate for mechanical stress by conferring plasticity to germ cell rachis bridges. To test whether ANI-2 can compensate for mechanical stress, we performed time-lapse imaging of the hermaphrodite gonad during ovulation, when the movement of a mature oocyte into the spermatheca causes deformation of the proximal gonad, and is therefore likely to cause mechanical stress on the gonad and rachis bridges (Fig. 8 A). The proximal ANI-2–enriched rachis in control animals displayed elastic properties, as it stretched to reach a maximum at the moment when the oocyte entered the spermatheca and decreased rapidly thereafter (Fig. 8, A and B; and Video 1). Interestingly, the diameter of the proximal-most rachis bridge also reached its maximum upon ovulation (Fig. 8 C). This indicates that the proximal gonad undergoes elastic deformation during ovulation and further suggests that changes in rachis bridge diameter permit this deformation.

As ANI-2 is enriched at rachis bridges and is required for their stability, we tested whether ANI-2 is required for deformation of the proximal gonad. In ovulating hermaphrodites partially depleted of ANI-2 by RNAi, the length of the proximal rachis remained stable and did not reach a maximum at the time of oocyte passage into the spermatheca (Fig. 8 B and Video 2). Accordingly, rachis bridges did not display a transient increase in diameter and remained constant throughout ovulation in these animals (Fig. 8 C). This indicates that ANI-2 is required for elastic deformation of the gonad during ovulation and further supports the notion that its enrichment at rachis bridges stabilizes these structures by permitting their deformation.

Discussion

In this study we showed that the primordial germ cells Z_2 and Z_3 do not share cytoplasmic connection and that the syncytial

Downloaded from jcb.rupress.org on July 9, 2017

architecture of the *C. elegans* germline arises progressively during larval development. The short Anillin ANI-2 is found in every germ cell, from birth of the two primordial germ cells during embryogenesis to oocyte cellularization when oogenesis completes. We demonstrated that ANI-2 is required to promote rachis bridge organization and that its absence leads to a collapse of membrane partitions between germ cells, and thus germ cell multinucleation, in part due to an increase in ANI-1 activity. We further provided evidence that this defect may be a consequence of cytoplasmic streaming in the rachis that initiates at the onset of oogenesis, and that ANI-2 can confer elastic properties to the rachis bridges when they are subjected to deformation. Based on these results, we propose a model (Fig. 8 D) in which the balance of activity between ANI-2 and ANI-1 at rachis bridges stabilizes these structures and provides them with the capacity to sustain the mechanical stress that results from cytoplasmic streaming in the gonad (and perhaps also ovulation), thus ensuring proper germline stability and organization.

Our finding that germ cell rachis bridges are not fully formed at the first larval stage and open progressively during larval development is consistent with observations made by electron microscopy that syncytial organization of the germline only becomes apparent at the L2 stage (Hirsh et al., 1976). Yet, we detected specific accumulation of ANI-2 in the P_4 blastomere and at the midbody between the two primordial germ cells. This supports a view in which the cortical loading and stabilization of ANI-2 upon division of P_4 contributes to prevent the completion of cytokinesis and serves as a nucleating event for intercellular bridge formation. The bridge between Z_2 and Z_3 would initially have a small diameter that would preclude cytoplasmic exchange between the two cells but would progressively increase its diameter during larval development. However, some of our results suggest that other regulators may contribute to intercellular bridge formation independently of ANI-2. First, whereas most germ cells in *ani-2* mutant L4 larvae have no detectable rachis bridge, 30% of them displayed a smaller but yet measurable opening to the rachis, indicating that some bridge formation can occur independently of ANI-2. Second, whereas rachis bridge diameter increased during larval development in wild-type animals, it remained small in these 30% of *ani-2* mutant germ cells, suggesting that ANI-2 promotes the opening of rachis bridges. Finally, we observed actin-dependent cytoplasmic streaming in the rachis of *ani-2* mutants, suggesting that actin cables, which are typically nucleated in the cytoplasm, can reach the central rachis, again arguing for the existence of at least small rachis bridges in *ani-2* mutants. This suggests that ANI-2 does not control the formation of rachis bridges, per se, but is required to promote their opening during larval development. Further experiments will be needed to resolve whether ANI-2 functions at one or more level of germline syncytial organization.

How does ANI-2 coordinate rachis bridge organization? ANI-2 is predicted to possess the C-terminal domains found in canonical Anillin and required for binding to RhoA, RacGAP50C (*Drosophila* MgcRacGAP), septins, and lipids of the plasma membrane, but to lack the N-terminal actin- and myosin-binding domains (Maddox et al., 2005). Accordingly, it was previously proposed to function as a negative regulator of contractility by competing with the canonical Anillin ANI-1 for one or more contractility regulators (Chartier et al., 2011). In support of this, we found that depletion of ANI-1 results in a number of germline defects opposite to those observed in ANI-2–depleted animals: when compared with wild-type animals, oocyte cellularization is delayed (as opposed to precocious in *ani-2(RNAi)* animals), the diameter of rachis bridges is larger (it is smaller in *ani-2* mutants), and rachis diameter is increased (it is decreased in *ani-2* mutants). Furthermore, depleting ANI-1 partially suppressed the defects observed in *ani-2* mutants. ANI-1 and ANI-2 did not control their respective loading at rachis bridges, suggesting that they function by locally balancing each other's activity. A balance of activity between ANI-1 and ANI-2 at rachis bridges could maintain the organization of these structures by locally controlling the engagement of contractility regulators, and thus regulate rachis bridge diameter. The progressive depletion of ANI-2 from rachis bridges would then promote oocyte cellularization, perhaps by allowing for more ANI-1 activity. However, depleting ANI-1 from *ani-2* mutant animals did not fully rescue their germ cell multinucleation phenotype, indicating that this defect does not arise solely from increased ANI-1 activity but likely involves other contractility regulators. Interestingly, ANI-2 was recently reported to promote the rachis bridge localization of the contractility regulators CYK-4/MgcRacGap and ZEN-4/MKLP1 (forming the centralspindlin complex), whose depletion results in a germline organization defect similar to that of *ani-2* mutants (Green et al., 2011; Zhou et al., 2013). We propose that ANI-2 regulates the lability of rachis bridges by locally controlling the activity of one or more contractility regulators, either by itself or by competing for their binding with the canonical Anillin ANI-1.

Intercellular bridges between germ cells are found in multiple organisms and were previously proposed to serve a number of possible functions, such as equilibrating gene products between haploid cells, synchronizing germ cell development, enabling the rapid transport of nutrients between cells, and homogenizing gamete quality (Dym and Fawcett, 1971; Guo and Zheng, 2004). Our findings that rachis bridge diameter increases as the rachis is stretched during ovulation and that ANI-2 is important to mediate elastic deformation suggests that intercellular bridges may additionally function to resist sustained mechanical stress. For instance, resistance to mechanical stress could be important for mammalian spermatogonia that migrate as germ cysts across Sertoli cell tight junctions during their maturation (Smith and Braun, 2012), a process that is likely to face great mechanical constraint. Actin-binding proteins, including Anillin, are found at intercellular bridges in many species, but it is currently unclear if a role for Anillin in regulating bridge stabilization is conserved. Interestingly, while a single gene encoding Anillin is present in humans, a shorter spliced isoform lacking the actin-binding domain is expressed in certain tissues (unpublished data). Shorter isoforms such as these could have a function similar to ANI-2 at intercellular bridges and thus play a role in regulated cytokinesis failure and/or intercellular bridge elasticity.

Downloaded from jcb.rupress.org on July 9, 2017

Materials and methods

Strains and alleles

All strains were maintained as described by Brenner (1974) and were grown at 20°C unless otherwise stated. The strains and alleles used in this study are listed in Table S1. Protein depletion by feeding RNAi was performed as described previously (Kamath et al., 2001) using the following individual clones from Julie Arhinger's library: sjj_K10B2.5 (*ani-2*), sjj_Y49E10.19 (*ani-1*), sjj_T05G5.3 (*cdk-1*), sjj_K06H7.1 (*plk-1*), sjj_T23G11.3 (*gld-1*), sjj_ZC308.1 (*gld-2*), sjj_M04B2.1 (*mep-1*), and sjj_Y49E10.14 (*pie-1*). In brief, each clone was grown up to log phase and plated overnight on NGM plates containing 50 µM carbenicillin and 1 mM IPTG. All assays were performed on animals grown in the presence of a dsRNA-expressing clone from the L1 stage (*ani-1* and *gld-1/2*) or the L4 stage (all other clones). All clones were verified by sequencing. A vector targeting a gene with no obvious function in embryogenesis or germline formation (sjj_C32E12.1; Chartier et al., 2011) was used as a control.

Transgenic animals expressing ANI-2 fused to GFP under the control of the *pie-1* promoter were generated by microparticle bombardment of a vector containing the complete *ani-2* coding region (amplified by PCR from genomic DNA) inserted in-frame downstream of sequence coding for GFP, a cleavage site for the TEV protease and S-peptide, as described previously (Cheeseman et al., 2004). The germline localization pattern of this fusion protein is indistinguishable from that observed on fixed specimen using anti–ANI-2 antibodies (Maddox et al., 2005).

The staging of animals during larval development was done according to growth parameters and gonad morphology (Fig. 2 B), using the following criteria. L1 stage: two germ cells (Z_2 and Z_3). L2 stage: multiple germ cells in a single gonad after 15–18 h of growth at 20°C. Early L3 stage: the gonad has split into anterior and posterior regions but the distal arms have not yet started to turn dorsally. Late L3 stage: both distal arms have turned dorsally but have not yet initiated looping. Early L4 stage: both distal arms have looped but the length of the distal arm is shorter than half that of the proximal arm. Mid L4 stage: the length of the distal arm equals half that of the proximal arm. Late L4 stage: the distal arm and proximal arms have the same length, yet no oocyte is visible. 20 and 48 h post-L4 stages: 68 h and 96 h, respectively, after providing food to synchronized L1 larvae at 20°C (animals were confirmed to be in late L4 stage by visual inspection after 48 h of feeding).

Immunofluorescence

To monitor ANI-2 localization, embryos were obtained after cutting open gravid hermaphrodites in 6 µl of M9 buffer with two 25-gauge needles on a 14 × 14-mm patterned Cel-Line slide (Thermo Fisher Scientific) coated with 0.1% poly-L-lysine. A coverslip was placed on the sample and the slide was placed for at least 5 min on a metal block cooled in dry ice. The coverslip was then removed and the slide was placed immediately in fixative (−20°C methanol) for 20 min. The slide was rehydrated twice with 1× PBS for 5 min, then once with 1× PBST (PBS with 0.1% Tween 20) for 5 min, and then incubated in blocking buffer (1× PBST containing 10% goat serum) for 30 min at room temperature. Antibodies were then applied in blocking buffer and incubated overnight at 4°C (primary) or 1 h at room temperature (secondary), each followed by four washes of 5 min in PBST. The fixed specimens were mounted in 90% glycerol containing 1% *N*-propyl gallate and a coverslip was sealed. Embryos were visualized with a laser-scanning confocal microscope (LSM 510; Carl Zeiss) equipped with a 63×/1.4 NA Plan Apochromat objective (Carl Zeiss). The following antibodies were used: rat anti–PAR-4 (1:50; Narbonne et al., 2010), rabbit anti–ANI-2 (1:1,000; Maddox et al., 2005), mouse clone DM1A anti–α-tubulin (1:500; Sigma-Aldrich), and mouse clone OIC1D4 anti-P granules (1:300; Developmental Studies Hybridoma Bank, University of Iowa, Iowa City, IA). Secondary antibodies were Alexa Fluor 488–coupled goat anti–rabbit, Alexa Fluor 647–coupled donkey anti–mouse (1:500 each; Invitrogen), and Cy3-conjugated donkey anti–rat (1:500; Jackson ImmunoResearch Laboratories, Inc.).

To visualize germ cell meiotic progression, gonads were extruded by cutting open young adult animals behind the pharynx in 1× PBS on poly-L-lysine–coated slides and immediately fixed in 1% paraformaldehyde for 5 min. A coverslip was placed on the sample and the slide was snap-frozen in liquid nitrogen. The coverslip was then removed and the slide was immerged in methanol at −20°C for 1 min. The slide was rehydrated with 1× PBST and incubated in blocking buffer (1× PBST containing 1% bovine serum albumin) for 1 h at room temperature. Primary and secondary antibodies were applied in blocking buffer and incubated overnight at room temperature, each followed by four washes of 5 min in PBST. The fixed specimens were mounted in Vectashield (Vector Laboratories) containing 1 µg/µl of DAPI and a coverslip was sealed. Images were acquired with CoolSnap HQ camera (Photometrics) mounted on a DeltaVision Image Restoration System (Applied Precision). A 100×/1.35 NA Plan Apochromat objective was used to acquire sections (separated by 0.2 µm) of the gonad, and image processing and deconvolution was done with softWoRx 3.0 software (Applied Precision). The primary antibodies were rabbit anti–HTP-3 (1:200; Goodyer et al., 2008) and guinea pig anti–SYP-1 (1:800; MacQueen et al., 2002). Secondary antibodies were Alexa Fluor 488–coupled goat anti–rabbit and Alexa Fluor 555–coupled goat anti–guinea pig (1:1,000 each; Invitrogen).

Fluorescence imaging of living animals

To analyze rachis length and rachis bridge diameter during ovulation, animals were mounted individually on a coverslip coated with 0.1% poly-L-lysine and were anaesthetized in 10 µl of egg buffer (Edgar, 1995) containing 0.1% tetramisole (Sigma-Aldrich). The coverslip was placed on a 3% agarose pad and the edges were sealed with petroleum jelly. Time-lapse movies were acquired with a CoolSnap HQ^2 camera (Photometrics) mounted on a swept field confocal microscope (Nikon and Prairie Technologies), using the 70-µm slit setting. A 60×/1.4 NA Plan Apochromat objective was used to acquire 29 confocal sections (separated by 0.5 µm) of the gonad, each exposed for 200 ms at 30-s intervals and with minimal laser power to avoid phototoxicity. All acquisition parameters and settings were controlled by Elements software (Nikon). Confocal sections are presented as maximal intensity projections of the entire stacks. The length of the proximal rachis, from gonad turn to the proximal tip, and the diameter of the most proximal rachis bridge were measured for each time point using ImageJ software (National Institutes of Health).

For analysis of rachis bridge formation, synchronized animals of a desired developmental stage were mounted and visualized with a swept field microscope as described above, except that the 35-µm slit and 60×/1.4 NA or 100×/1.4 NA objectives were used to acquire confocal sections (separated by 0.5 µm) spanning the entire rachis. When required, different regions of the gonad were acquired separately and reconstructed in a single image using the Photomerge function in Adobe Photoshop. To monitor rachis bridges, six consecutive confocal sections were analyzed independently using ImageJ, by measuring fluorescence intensity of expressed fluorescent markers along a 3-pixel-thick line drawn along the lateral and apical cortex, as depicted in Fig. 2 C. Mean fluorescence intensity profiles of each marker were represented along the cortical perimeter. Rachis bridge diameter was determined by measuring the maximal distance between the peaks of fluorescent markers in all analyzed confocal sections. For GFP::ANI-2, GFP::ANI-1, and NMY-2::GFP, peaks were defined as pixels with maximum intensity across the whole fluorescence profile. Distinct peaks were defined as two distinct intensity maximums separated by at least 0.8 µm. For the membrane marker, the fluorescence intensity minimum was defined as the single pixel in the curve with the lowest fluorescence intensity. Peaks were defined as the first measured local maximums of fluorescence intensity, on each side of the minimum, that were maintained over three consecutive pixels and separated by at least 0.8 µm.

To visualize membrane partition collapse between germ cells, L4-stage or young adult animals were mounted and visualized with a swept field microscope as described above, and the 60×/1.4 NA objective was used to acquire 29 confocal sections (separated by 0.75 µm) every 30 s. We could only ascribe two clear membrane collapse events, largely due to several limitations in our experimental conditions: (1) we performed imaging in every region of the gonad; however, imaging was done at high magnification and each time-lapse acquisition encompassed only a small portion of a gonad arm, thus excluding collapse events occurring in regions not being examined during the analysis; (2) while time-lapse acquisitions were done in multiple confocal sections, we felt confident to ascribe a collapse event only when it occurred in germ cells with their nuclei in the same mid-section plane of the gonad; we observed six additional collapse events but the fact that they were occurring more or less along the z-plane made it more difficult to unambiguously ascribe them as such; this is even further exacerbated by the fact that the germline of *ani-2* mutants is disorganized and therefore many germ cell nuclei are not found in a single mid-section plane; and (3) membrane collapsing is an event that is likely very rapid and may occur at a frequency beyond the duration of our acquisition time (40 min).

Kymograph analysis of cytoplasmic streaming in the rachis

Living animals were mounted and immobilized as described above. Cytoplasmic movement in the rachis was visualized by differential interference

Downloaded from jcb.rupress.org on July 9, 2017

contrast microscopy, using an HRM camera (Carl Zeiss) mounted on a microscope (Axio Imager Z1; Carl Zeiss). Mid-section images of the rachis were acquired with a Plan Apochromat 63×/1.4 NA objective at 15-s intervals. Kymographs of cytoplasmic movement in the rachis were generated using the multiple kymograph plug-in available for ImageJ, by visualizing particle displacement over time along a 7-pixel-wide line drawn from the pachytene region to the proximal end of the gonad. The velocity of cytoplasmic streaming was obtained by averaging the speed of at least 25 particles moving around the loop region of each gonad.

Rhodamine-dextran photoactivation

Tetramethylrhodamine-labeled dextran (10 kD; Molecular Probes) was reconstituted to 1 mg/ml in injection buffer (1 mM potassium citrate, 6.7 mM KPO_4, pH 7.5, and 0.67% PEG) and injected into the gonad of adult JH2107 animals (expressing GFP::PGL-1, to visualize the primordial germ cells). After 12 h, embryos were obtained by cutting open the injected gravid hermaphrodites using two 25-gauge needles and mounted individually on a coverslip coated with 0.1% poly-L-lysine in 10 µl of egg buffer. The coverslip was placed on a 3% agarose pad and the edges were sealed with petroleum jelly. Photoactivation in one of the two primordial germ cells was performed with a 405-nm laser mounted on a confocal microscope (LSM 510; Carl Zeiss) equipped with a 63×/1.4 NA Plan Apochromat objective, and fluorescence was monitored after excitation with a 543-nm laser. Fluorescence intensities were measured using ImageJ software in the photoactivated primordial germ cell, its non-photoactivated sister, and a control neighboring somatic cell.

Statistical analysis

Statistical significance between samples was performed by applying Student's *t* test using Microsoft Excel. Assumptions of normality and equal variance were met for all data analyzed. A two-tailed p-value smaller than 0.05 was considered significant. All results are expressed as average ± SD. Sample size (*n*) and p-values are given on each figure panel or in the figure legends.

Online supplemental material

Fig. S1 shows that ANI-1 and NMY-2 localize to the rachis of wild-type hermaphrodites and report on rachis bridge organization. Fig. S2 shows that fluorescent dextran diffuses rapidly in the cytoplasm of an embryonic blastomere. Fig. S3 shows additional evidence that ANI-2 is required for rachis bridge stability. Fig. S4 provides additional details on the phenotypic characterization of *ani-2* mutant animals. Video 1 shows time-lapse analysis of gonad elastic deformation during ovulation in a wild-type hermaphrodite. Video 2 shows time-lapse analysis of gonad elastic deformation during ovulation in a hermaphrodite partially depleted of ANI-2. Table S1 lists the strains and alleles used in this study. Online supplemental material is available at http://www.jcb.org/cgi/content/full/jcb.201310117/DC1.

We are grateful to Karen Oegema, Patrick Narbonne, the Japanese *C. elegans* Gene Knockout Consortium, and the *Caenorhabditis* Genetics Center for strains and reagents. We also thank Paul Maddox, Abby Gerhold, Jonas Dorn, Joel Ryan, Benjamin Lacroix, and members of the Maddox and Labbé laboratories for helpful discussions and comments on the manuscript; and Christian Charbonneau of the Institute of Research in Immunology and Cancer's (IRIC) Bio-imaging Facility for technical help with image acquisition.

A.S. Maddox was supported by salary awards from the Fonds de Recherche du Québec en Santé (FRQS) and the Canadian Institutes of Health Research (CIHR). N.T. Chartier was a research fellow of the FRQS and holds a fellowship from the Fondation pour la Recherche Médicale (France). This work was funded by grants from the National Science and Engineering Research Council of Canada (#434942) and the CIHR (MOP-111142) to J.-C. Labbé, who holds the Canada Research Chair in Cell Division and Differentiation. IRIC is supported in part by the Canadian Center of Excellence in Commercialization and Research, the Canada Foundation for Innovation, and the FRQS.

The authors declare no competing financial interests.

Submitted: 25 October 2013
Accepted: 2 June 2014

References

Brenner, S. 1974. The genetics of *Caenorhabditis elegans*. *Genetics*. 77:71–94.

Brill, J.A., G.R. Hime, M. Scharer-Schuksz, and M.T. Fuller. 2000. A phospholipid kinase regulates actin organization and intercellular bridge formation during germline cytokinesis. *Development*. 127:3855–3864.

Chartier, N.T., D.P. Salazar Ospina, L. Benkemoun, M. Mayer, S.W. Grill, A.S. Maddox, and J.C. Labbé. 2011. PAR-4/LKB1 mobilizes nonmuscle myosin through anillin to regulate *C. elegans* embryonic polarization and cytokinesis. *Curr. Biol.* 21:259–269. http://dx.doi.org/10.1016/j.cub.2011.01.010

Cheeseman, I.M., S. Niessen, S. Anderson, F. Hyndman, J.R. Yates III, K. Oegema, and A. Desai. 2004. A conserved protein network controls assembly of the outer kinetochore and its ability to sustain tension. *Genes Dev.* 18:2255–2268. http://dx.doi.org/10.1101/gad.1234104

Deppe, U., E. Schierenberg, T. Cole, C. Krieg, D. Schmitt, B. Yoder, and G. von Ehrenstein. 1978. Cell lineages of the embryo of the nematode *Caenorhabditis elegans*. *Proc. Natl. Acad. Sci. USA*. 75:376–380. http://dx.doi.org/10.1073/pnas.75.1.376

Dym, M., and D.W. Fawcett. 1971. Further observations on the numbers of spermatogonia, spermatocytes, and spermatids connected by intercellular bridges in the mammalian testis. *Biol. Reprod.* 4:195–215.

Edgar, L.G. 1995. Blastomere culture and analysis. *Methods Cell Biol.* 48:303–321. http://dx.doi.org/10.1016/S0091-679X(08)61393-X

Field, C.M., and B.M. Alberts. 1995. Anillin, a contractile ring protein that cycles from the nucleus to the cell cortex. *J. Cell Biol.* 131:165–178. http://dx.doi.org/10.1083/jcb.131.1.165

Francis, R., M.K. Barton, J. Kimble, and T. Schedl. 1995. *gld-1*, a tumor suppressor gene required for oocyte development in *Caenorhabditis elegans*. *Genetics*. 139:579–606.

Goodyer, W., S. Kaitna, F. Couteau, J.D. Ward, S.J. Boulton, and M. Zetka. 2008. HTP-3 links DSB formation with homolog pairing and crossing over during *C. elegans* meiosis. *Dev. Cell*. 14:263–274. http://dx.doi.org/10.1016/j.devcel.2007.11.016

Green, R.A., H.L. Kao, A. Audhya, S. Arur, J.R. Mayers, H.N. Fridolfsson, M. Schulman, S. Schloissnig, S. Niessen, K. Laband, et al. 2011. A high-resolution *C. elegans* essential gene network based on phenotypic profiling of a complex tissue. *Cell*. 145:470–482. http://dx.doi.org/10.1016/j.cell.2011.03.037

Green, R.A., J.R. Mayers, S. Wang, L. Lewellyn, A. Desai, A. Audhya, and K. Oegema. 2013. The midbody ring scaffolds the abscission machinery in the absence of midbody microtubules. *J. Cell Biol.* 203:505–520. http://dx.doi.org/10.1083/jcb.201306036

Greenbaum, M.P., W. Yan, M.H. Wu, Y.N. Lin, J.E. Agno, M. Sharma, R.E. Braun, A. Rajkovic, and M.M. Matzuk. 2006. TEX14 is essential for intercellular bridges and fertility in male mice. *Proc. Natl. Acad. Sci. USA*. 103:4982–4987. http://dx.doi.org/10.1073/pnas.0505123103

Greenbaum, M.P., T. Iwamori, G.M. Buchold, and M.M. Matzuk. 2011. Germ cell intercellular bridges. *Cold Spring Harb. Perspect. Biol.* 3:a005850. http://dx.doi.org/10.1101/cshperspect.a005850

Guo, G.Q., and G.C. Zheng. 2004. Hypotheses for the functions of intercellular bridges in male germ cell development and its cellular mechanisms. *J. Theor. Biol.* 229:139–146. http://dx.doi.org/10.1016/j.jtbi.2004.03.010

Haglund, K., I.P. Nezis, and H. Stenmark. 2011. Structure and functions of stable intercellular bridges formed by incomplete cytokinesis during development. *Commun. Integr. Biol.* 4:1–9.

Hall, D.H., V.P. Winfrey, G. Blaeuer, L.H. Hoffman, T. Furuta, K.L. Rose, O. Hobert, and D. Greenstein. 1999. Ultrastructural features of the adult hermaphrodite gonad of *Caenorhabditis elegans*: relations between the germ line and soma. *Dev. Biol.* 212:101–123. http://dx.doi.org/10.1006/dbio.1999.9356

Hirsh, D., D. Oppenheim, and M. Klass. 1976. Development of the reproductive system of *Caenorhabditis elegans*. *Dev. Biol.* 49:200–219. http://dx.doi.org/10.1016/0012-1606(76)90267-0

Kachur, T.M., A. Audhya, and D.B. Pilgrim. 2008. UNC-45 is required for NMY-2 contractile function in early embryonic polarity establishment and germline cellularization in *C. elegans*. *Dev. Biol.* 314:287–299. http://dx.doi.org/10.1016/j.ydbio.2007.11.028

Kamath, R.S., M. Martinez-Campos, P. Zipperlen, A.G. Fraser, and J. Ahringer. 2001. Effectiveness of specific RNA-mediated interference through ingested double-stranded RNA in *Caenorhabditis elegans*. *Genome Biol*. 2:RESEARCH0002. http://dx.doi.org/10.1186/gb-2000-2-1-research0002

Kawasaki, I., Y.H. Shim, J. Kirchner, J. Kaminker, W.B. Wood, and S. Strome. 1998. PGL-1, a predicted RNA-binding component of germ granules, is essential for fertility in *C. elegans*. *Cell*. 94:635–645. http://dx.doi.org/10.1016/S0092-8674(00)81605-0

Kim, S., C. Spike, and D. Greenstein. 2013. Control of oocyte growth and meiotic maturation in *Caenorhabditis elegans*. *Adv. Exp. Med. Biol.* 757:277–320. http://dx.doi.org/10.1007/978-1-4614-4015-4_10

Kimble, J., and S.L. Crittenden. 2007. Controls of germline stem cells, entry into meiosis, and the sperm/oocyte decision in *Caenorhabditis elegans*. *Annu. Rev. Cell Dev. Biol.* 23:405–433. http://dx.doi.org/10.1146/annurev.cellbio.23.090506.123326

Downloaded from jcb.rupress.org on July 9, 2017

Lacroix, B., and A.S. Maddox. 2012. Cytokinesis, ploidy and aneuploidy. *J. Pathol.* 226:338–351. http://dx.doi.org/10.1002/path.3013

MacQueen, A.J., M.P. Colaiácovo, K. McDonald, and A.M. Villeneuve. 2002. Synapsis-dependent and -independent mechanisms stabilize homolog pairing during meiotic prophase in *C. elegans*. *Genes Dev.* 16:2428–2442. http://dx.doi.org/10.1101/gad.1011602

Maddox, A.S., B. Habermann, A. Desai, and K. Oegema. 2005. Distinct roles for two *C. elegans* anillins in the gonad and early embryo. *Development*. 132:2837–2848. http://dx.doi.org/10.1242/dev.01828

Maddox, A.S., L. Lewellyn, A. Desai, and K. Oegema. 2007. Anillin and the septins promote asymmetric ingression of the cytokinetic furrow. *Dev. Cell*. 12:827–835. http://dx.doi.org/10.1016/j.devcel.2007.02.018

McCarter, J., B. Bartlett, T. Dang, and T. Schedl. 1999. On the control of oocyte meiotic maturation and ovulation in *Caenorhabditis elegans*. *Dev. Biol.* 205:111–128. http://dx.doi.org/10.1006/dbio.1998.9109

Merritt, C., D. Rasoloson, D. Ko, and G. Seydoux. 2008. 3′ UTRs are the primary regulators of gene expression in the *C. elegans* germline. *Curr. Biol.* 18:1476–1482. http://dx.doi.org/10.1016/j.cub.2008.08.013

Nance, J., E.M. Munro, and J.R. Priess. 2003. *C. elegans* PAR-3 and PAR-6 are required for apicobasal asymmetries associated with cell adhesion and gastrulation. *Development*. 130:5339–5350. http://dx.doi.org/10.1242/dev.00735

Narbonne, P., V. Hyenne, S. Li, J.C. Labbé, and R. Roy. 2010. Differential requirements for STRAD in LKB1-dependent functions in *C. elegans*. *Development*. 137:661–670. http://dx.doi.org/10.1242/dev.042044

Oegema, K., M.S. Savoian, T.J. Mitchison, and C.M. Field. 2000. Functional analysis of a human homologue of the *Drosophila* actin binding protein anillin suggests a role in cytokinesis. *J. Cell Biol.* 150:539–552. http://dx.doi.org/10.1083/jcb.150.3.539

Paoletti, A., and F. Chang. 2000. Analysis of mid1p, a protein required for placement of the cell division site, reveals a link between the nucleus and the cell surface in fission yeast. *Mol. Biol. Cell*. 11:2757–2773. http://dx.doi.org/10.1091/mbc.11.8.2757

Smith, B.E., and R.E. Braun. 2012. Germ cell migration across Sertoli cell tight junctions. *Science*. 338:798–802. http://dx.doi.org/10.1126/science.1219969

Straight, A.F., C.M. Field, and T.J. Mitchison. 2005. Anillin binds nonmuscle myosin II and regulates the contractile ring. *Mol. Biol. Cell*. 16:193–201. http://dx.doi.org/10.1091/mbc.E04-08-0758

Sulston, J.E., E. Schierenberg, J.G. White, and J.N. Thomson. 1983. The embryonic cell lineage of the nematode *Caenorhabditis elegans*. *Dev. Biol.* 100:64–119. http://dx.doi.org/10.1016/0012-1606(83)90201-4

Wang, J.T., and G. Seydoux. 2013. Germ cell specification. *Adv. Exp. Med. Biol.* 757:17–39. http://dx.doi.org/10.1007/978-1-4614-4015-4_2

Wolke, U., E.A. Jezuit, and J.R. Priess. 2007. Actin-dependent cytoplasmic streaming in *C. elegans* oogenesis. *Development*. 134:2227–2236. http://dx.doi.org/10.1242/dev.004952

Zhou, K., M.M. Rolls, and W. Hanna-Rose. 2013. A postmitotic function and distinct localization mechanism for centralspindlin at a stable intercellular bridge. *Dev. Biol.* 376:13–22. http://dx.doi.org/10.1016/j.ydbio.2013.01.020

Downloaded from jcb.rupress.org on July 9, 2017

Amini et al., http://www.jcb.org/cgi/content/full/jcb.201310117/DC1

THE JOURNAL OF CELL BIOLOGY

Figure S1. **ANI-1 and NMY-2 localize to the rachis of wild-type hermaphrodites and report on rachis bridge organization.** (A and D) Mid-section confocal images of the germline of wild-type early L3 (top), L4 (middle), and adult (bottom) hermaphrodites coexpressing a membrane marker and GFP::ANI-1 (A) or NMY-2::GFP (D). In all frames, anterior is to the left. Bars, 10 µm. (B and E) Proportion of germ cells showing rachis bridges with a diameter >0.8 µm (turquoise) or <0.8 µm (red) throughout development, as measured by GFP::ANI-1 (B) and NMY-2::GFP (E) fluorescence distribution. (C and F) Maximal rachis bridge diameter in germ cells of animals in various developmental stages, as measured with fluorescence distribution of the membrane marker (red) and GFP::ANI-1 (C, green) or NMY-2::GFP (F, green). Error bars represent SD. In B, C, E, and F, the numbers in brackets represent the total number of germ cells analyzed. The results on rachis bridge organization obtained with these markers are identical to those obtained after analysis of GFP::ANI-2 (Fig. 3).

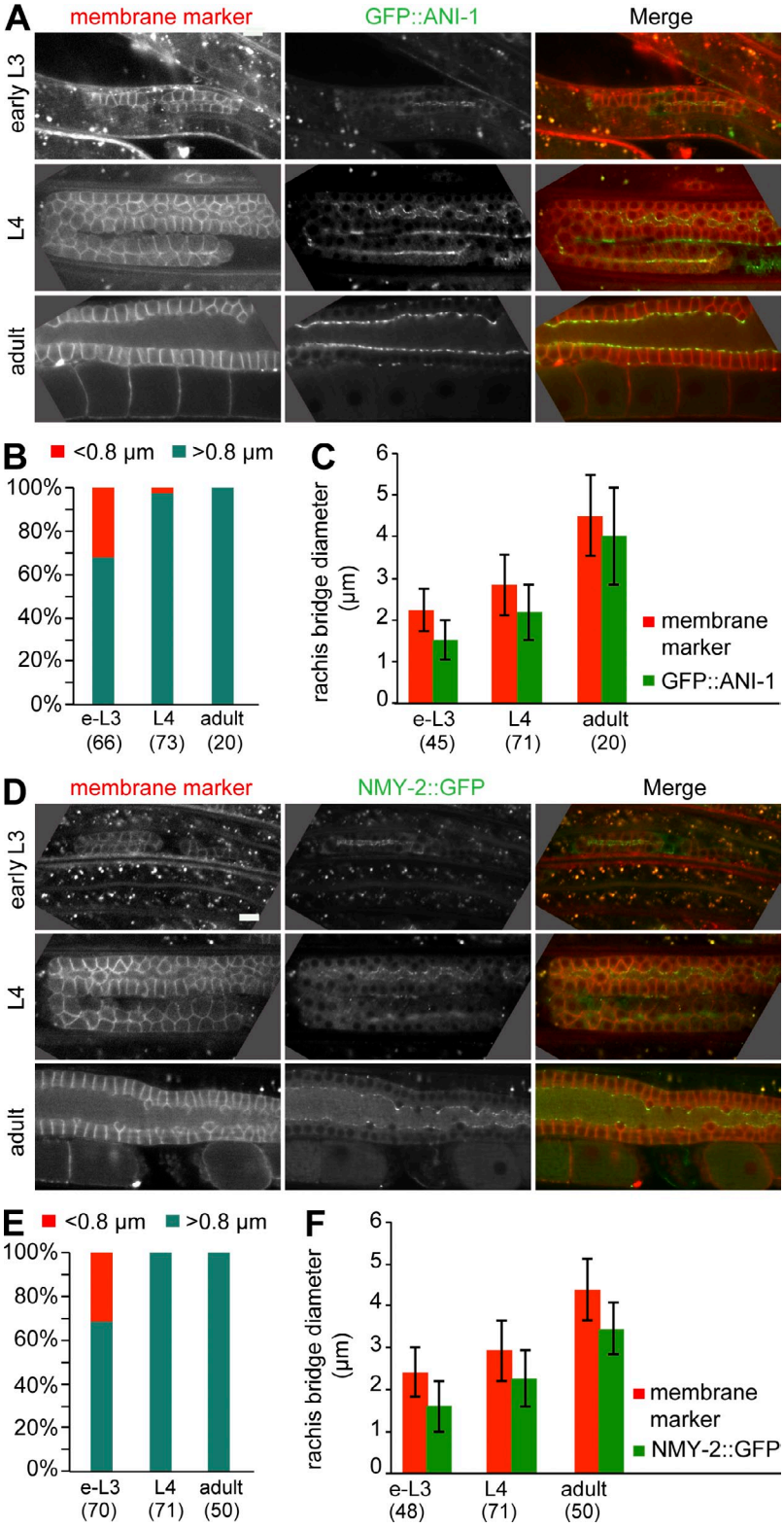

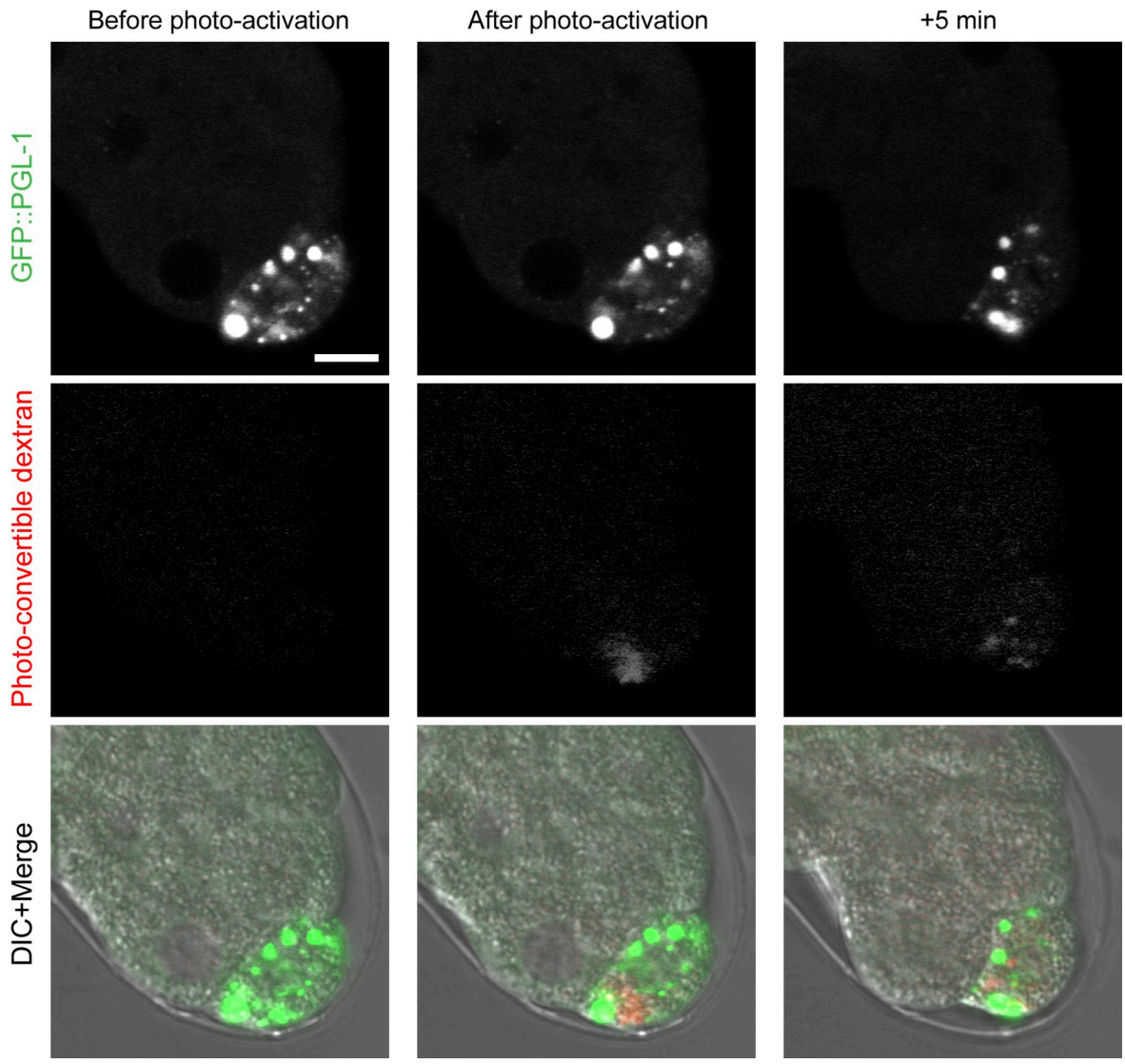

Figure S2. **Molecule diffusion in the cytoplasm of embryonic blastomeres.** Mid-section confocal images of an embryo expressing GFP::PGL-1 exogenously supplied with photo-convertible rhodamine-dextran. After photoactivation in part of the P_3 blastomere, the fluorescent signal rapidly spread throughout the cell. Bar, 10 μm.

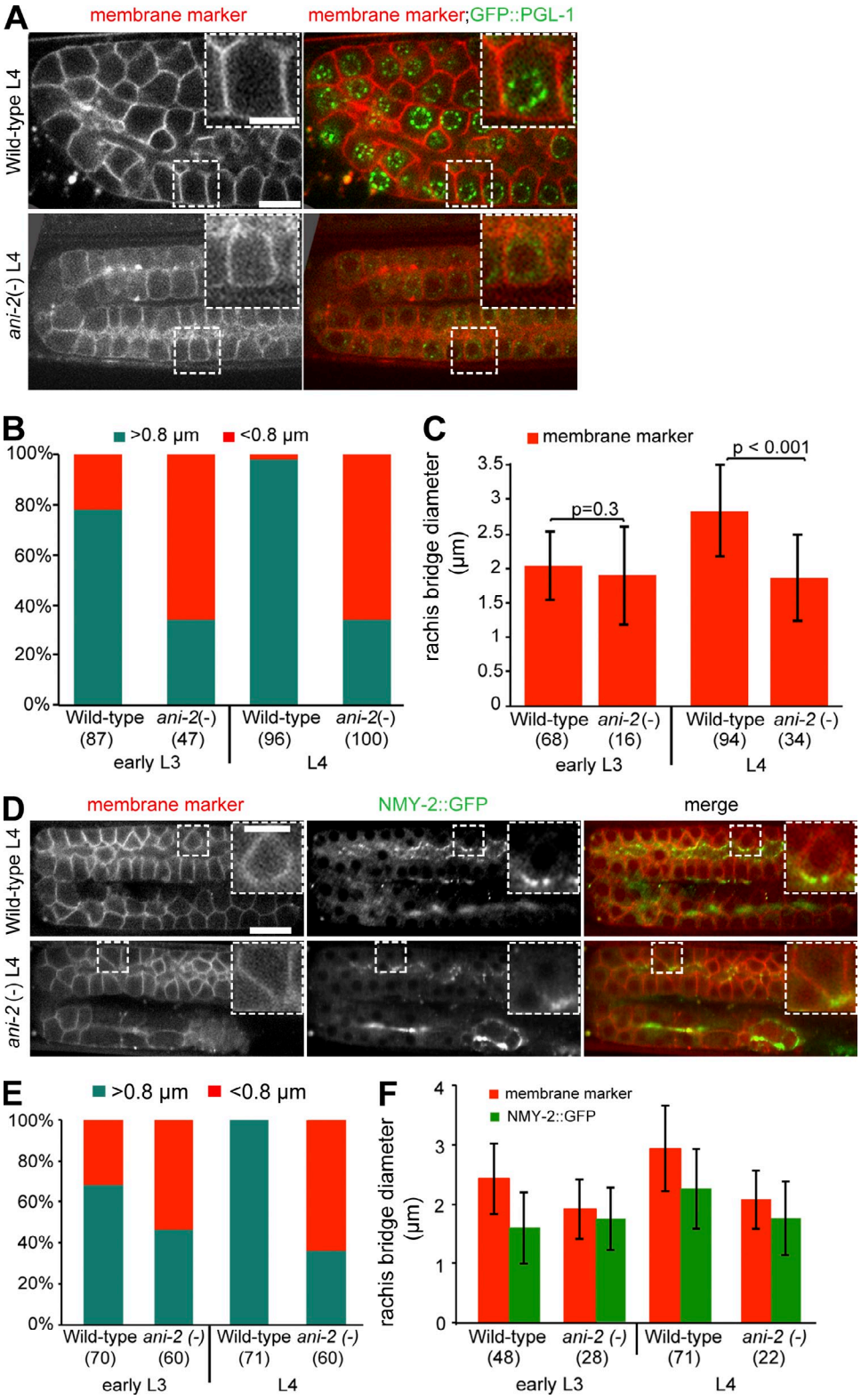

Figure S3. **ANI-2 is required for rachis bridge stability.** (A and D) Mid-section confocal images of the germline of a wild-type and an *ani-2*(−) L4 hermaphrodite expressing a membrane marker (red) and GFP::PGL-1 (A, green) or NMY-2::GFP (D, green). Bar, 10 µm. The regions delineated by the white dashed square are magnified in the inset (bar for insets, 5 µm). (B and E) Proportion of germ cells showing rachis bridges with a diameter >0.8 µm (turquoise) or <0.8 µm (red) in wild-type and *ani-2*(−) animals at the L3 and L4 larval stages, as measured by distribution of the membrane marker alone (B) or together with NMY-2::GFP (E). (C and F) Maximal rachis bridge diameter in germ cells of wild-type and *ani-2*(−) animals at the L3 and L4 larval stages, as measured with distribution of the membrane marker alone (red) or together with NMY-2::GFP (green). Rachis bridges that are <0.8 µm in diameter are excluded from this analysis. Error bars represent SD. In B, C, E, and F the numbers in brackets represent the total number of germ cells analyzed. The results on rachis bridge organization obtained with these markers are identical to those obtained after analysis of GFP::ANI-1 (Fig. 4).

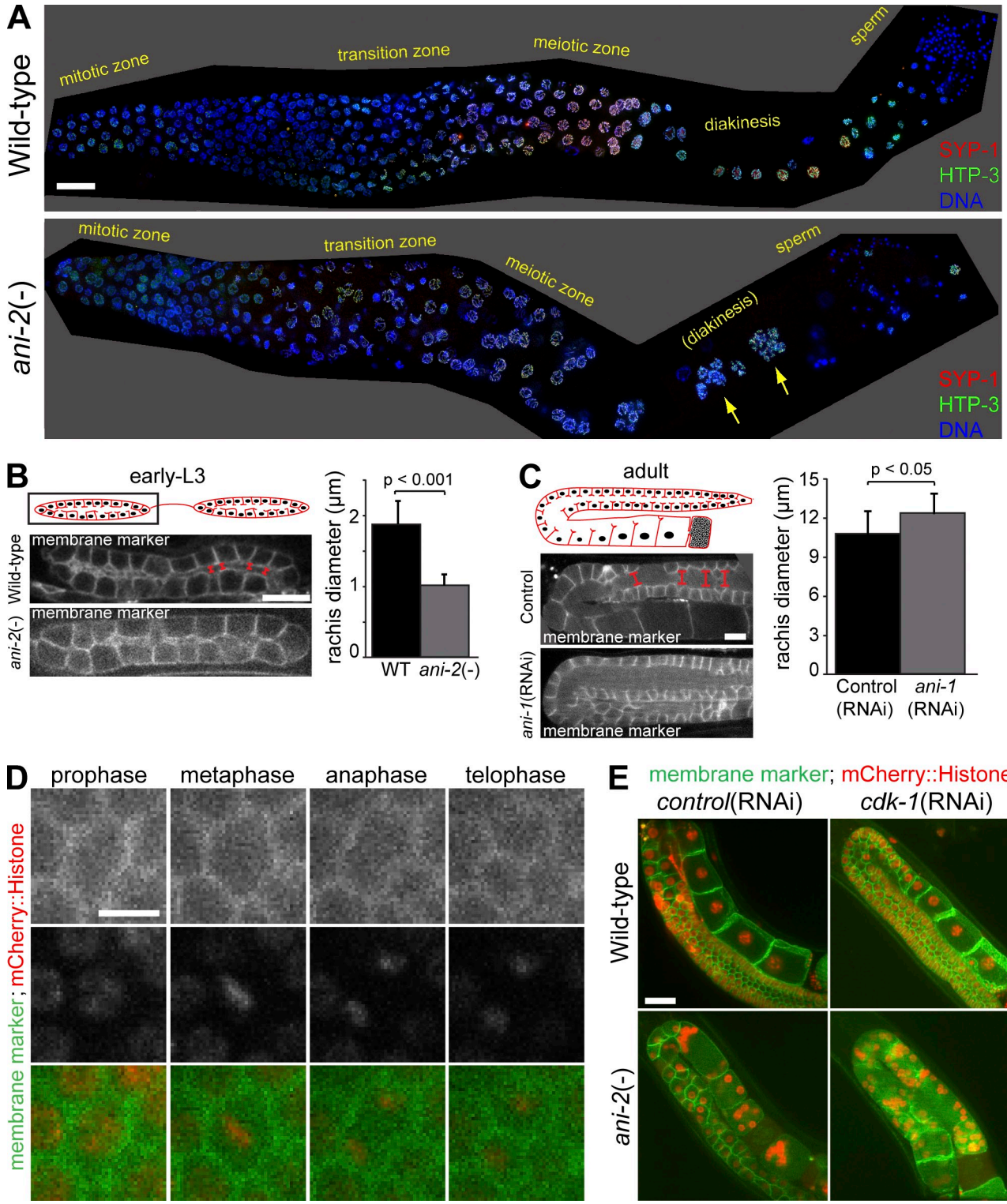

Figure S4. **Phenotypic analysis of *ani-2* mutants.** (A) Projected image stacks of fixed extruded gonads from wild-type (left) and *ani-2*(−) young adult hermaphrodites immunostained with SYP-1 (red), HTP-3 (green), and DAPI (blue). Arrows point to germ cells with defect in diakinesis. Each image was assembled from multiple acquisitions of the same gonad. Bar, 20 µm. (B) Schematic representation of the gonad and images of one gonad in wild-type and *ani-2*(−) mutant early L3 stage larvae. Rachis diameter was measured in multiple regions and confocal sections of the gonad (red line). The graph represents the average diameter of the rachis in wild-type and *ani-2*(−) mutant L3 stage larvae. Rachis diameter is significantly reduced in *ani-2*(−) mutants compared with the wild type. (C) Schematic representation of the gonad and images of one gonad in control and *ani-1(RNAi)* adult animals. Figure elements are as in B. Rachis diameter is significantly increased in *ani-1(RNAi)* animals compared with control. (D) Time-lapse confocal images of a germline stem cell dividing in the gonad of an *ani-2*(−) hermaphrodite. The cell properly progresses through all stages of M phase. Bar, 5 µm. (E) Mid-section confocal images of the germline of wild-type and *ani-2*(−) adult hermaphrodites expressing a membrane marker (green) and mCherry::Histone H2B (red). Blocking cell cycle progression with *cdk-1(RNAi)* (right) did not preclude germ cell multinucleation, indicating that it is not a consequence of inappropriate reentry into the cell cycle. Bar, 10 µm.

Video 1. **Analysis of gonad elastic deformation during ovulation in a wild-type hermaphrodite.** Time-lapse movie of the gonad of a wild-type hermaphrodite expressing GFP::ANI-2 (green) and a membrane marker (red) captured during ovulation. Images were captured every 30 s with a swept field confocal microscope (Nikon), and maximal-intensity projections are played at 10 images/s.

Video 2. **Analysis of gonad elastic deformation during ovulation in a hermaphrodite partially depleted of ANI-2.** Time-lapse movie of the gonad of a hermaphrodite partially depleted of ANI-2 and expressing GFP::ANI-2 (green) and a membrane marker (red) captured during ovulation. Images were captured every 30 s with a swept field confocal microscope (Nikon), and maximal-intensity projections are played at 10 images/s.

Table S1. ***C. elegans* strains used in this study**

Strain no.	Genotype
N2	Wild-type Bristol strain
VC703	*ani-2(ok1147)/mIn1[mIs14 dpy-10(e128)] II*
OD95	*unc-119(ed3) III; ltIs37 [Ppie-1::mCherry::his-58; unc-119(+)] IV; ltIs38 [Ppie-1::gfp::PH(PLC1delta1); unc-119(+)]*
UM185	*unc-119(ed3) III; ltIs44 [Ppie-1::mCherry::PH(PLC1delta1); unc-119(+)] IV; axIs1720 [Ppie-1::gfp::pgl-1::pgl-1 3′; unc-119(+)]*
UM186	*ani-2(ok1147)/mIn1[mIs14 dpy-10(e128)] II; ltIs44 [Ppie-1::mCherry::PH(PLC1delta1); unc-119(+)] IV; axIs1720 [Ppie-1::gfp::pgl-1::pgl-1 3′; unc-119(+)]*
UM208	*unc-119(ed3) III; ltIs81 [Ppie-1::gfp-TEV-Stag::ani-2; unc-119 (+)]; ltIs44 [Ppie-1::mCherry::PH(PLC1delta1); unc-119(+)] IV*
OD182	*unc-119(ed3) III; ltIs28 [Ppie-1::gfp-TEV-Stag::ani-1; unc-119 (+)]; ltIs44 [Ppie-1::mCherry::PH(PLC1delta1); unc-119(+)] IV*
UM341	*ani-2(ok1147)/mIn1[mIs14 dpy-10(e128)] II; unc-119(ed3) III; ltIs28 [Ppie-1::gfp-TEV-Stag::ani-1; unc-119 (+)]; ltIs44 [Ppie-1::mCherry::PH(PLC1delta1); unc-119(+)] IV*
OD183	*unc-119(ed3) III; ltIs44 [Ppie-1::mCherry::PH(PLC1delta1); unc-119(+)] IV; zuIs45 [Pnmy-2::nmy-2::gfp; unc-119 (+)] V*
UM342	*ani-2(ok1147)/mIn1[mIs14 dpy-10(e128)] II; unc-119(ed3) III; ltIs44 [Ppie-1::mCherry::PH(PLC1delta1); unc-119(+)] IV; zuIs45 [Pnmy-2::nmy-2::gfp; unc-119 (+)] V*
JH2107	*unc-119(ed3) III; axIs1720 [Ppie-1::gfp::pgl-1::pgl-1 3′; unc-119(+)]*
UM209	*ani-2(ok1147)/mIn1[mIs14 dpy-10(e128)] II; ltIs37 [Ppie-1::mCherry::his-58; unc-119(+)] IV; ltIs38 [Ppie-1::gfp::PH(PLC1delta1); unc-119(+)]*
JK2879	*gld-2(q497) gld-1(q485) I/hT2[qIs48] (I;III)*
UM230	*gld-2(q497) gld-1(q485) I/hT2[qIs48] (I;III); ani-2(ok1147)/mIn1[mIs14 dpy-10(e128)] II; ltIs37 [Ppie-1::mCherry::his-58; unc-119(+)] IV; ltIs38 [Ppie-1::gfp::PH(PLC1delta1); unc-119(+)]*